The Emission, Transport, and Impacts of the Extreme Saharan Dust Storm in 2015

Brian Harr, Bing Pu, Qinjian Jin

Department of Geography and Atmospheric Science, University of Kansas, Lawrence, KS, 66045, United States

Correspondence to: Brian Harr (bharr125@ku.edu), Bing Pu (bpu@ku.edu)

Abstract. Each summer, the Saharan Air Layer transports massive amounts of mineral dust across the Atlantic Ocean, affecting weather, climate, and public health over large areas. Despite the considerable impacts of African dust, the causes and impacts of extreme trans-Atlantic African dust events are not fully understood. The "Godzilla" trans-Atlantic dust event in 2020 has been extensively studied, but little is known about other similar events. Here we examine the June 2015 event, the second strongest trans-Atlantic African dust event during summers over 2003–2022. This event was characterized by moderately high dust emissions over western North Africa and an extremely high aerosol optical depth (AOD) over the tropical North Atlantic. The high dust loading over the Atlantic is associated with atmospheric circulation extremes like the "Godzilla" event. Both the African easterly jet (AEJ) and Caribbean low-level jet (CLLJ) are greatly intensified, along with a westward extension of the North Atlantic subtropical high (NASH), all of which favor the westward transport of African dust. The enhanced dust emissions are related to anomalously strong surface winds in dust source regions and reduced vegetation density and soil moisture over the northern Sahel.

The dust plume reduced surface net shortwave radiation over the eastern tropical North Atlantic by about 25 W m^{-2} but increased net longwave flux by about 3 W m^{-2}. In contrast to the "Godzilla" event, the 2015 event had minor air quality impacts on the U.S., partially due to the extremely intensified CLLJ that dispersed the dust plume to the Pacific.

1 Introduction

North Africa is the world's largest source of dust, emitting about 400 – 2200 Tg of mineral dust each year (e.g., Goudie and Middleton 2001; Huneeus et al. 2011; Wu et al. 2020; Kok et al. 2021). African dust aerosols can affect the Earth's radiation budget (e.g., Prospero and Lamb, 2003; Li et al., 2004; Engelstaedter et al., 2006; Schepanski, 2018; Francis et al., 2022), modify cloud properties by serving as cloud condensation nuclei and ice nuclei (Levin et al., 1996; Rosenfeld et al., 2001; Goudie and Middleton, 2001; DeMott et al., 2003; Prenni et al., 2009), and couple with global biogeochemical cycles when depositing vital mineral nutrients over land and ocean (Okin et al., 2004; Bristow et al., 2010; Kumar et al., 2014; Yu et al.,

2015b; Jickells et al., 2016; Villar-Argaiz et al., 2018). Climate change is expected to have major impacts on North Africa (Prospero et al., 2021), making it more pressing to understand the spatiotemporal variability of African dust and its associated impacts.

Each boreal summer a large amount of African dust is transported westward to the Atlantic Ocean. The thick, warm, and dry African dust plumes, namely the Saharan Air Layer (SAL; Carlson and Prospero 1972; Prospero and Carlson 1972; Karyampudi and Carlson 1988; Kanitz et al. 2014), can often propagate across the tropical North Atlantic to the Caribbean Basin and the southeastern U.S., affecting weather and climate systems along their transport pathways (e.g., Karyampudi and Carlson, 1988; Dunion and Velden, 2004; Jenkins et al., 2008; Strong et al., 2018). While much of the research seeks to understand the conditions associated with African dust emissions and westward transport and to quantitatively characterize the trans-Atlantic African dust plumes (Prospero and Lamb, 2003; Kaufman et al., 2005; Engelstaedter et al., 2006; Kalashnikova and Kahn, 2008; Knippertz and Todd, 2012; Fiedler et al., 2015; Yu et al., 2015b, 2019), only a small body of research is dedicated to examining the summertime extreme trans-Atlantic dust events, i.e., events with extremely high dust loading over the tropical North Atlantic (Huang et al. 2010; Francis et al. 2020; Yu et al. 2021; Pu and Jin 2021). The record-breaking trans-Atlantic African dust event in June 2020, namely, the "Godzilla" dust storm, is the strongest trans-Atlantic dust event in summertime since 2003 (Yu et al., 2021; Pu and Jin, 2021) and has been extensively studied (Francis et al., 2020; Yu et al., 2021; Pu and Jin, 2021; Francis et al., 2022; Scott et al., 2022; Asutosh et al., 2022; Mehra et al., 2023). It is found that the event is associated with both enhanced dust emissions over North Africa and intensified westward transport of dust related to circulation extremes (Yu et al., 2021; Pu and Jin, 2021). However, little is known about other similar extreme trans-Atlantic African dust events in summer. It is not clear what the major causes of the extremely high loading of African dust over the tropical North Atlantic are, e.g., whether mechanisms found in the 2020 event also apply to other events, and whether they resulted in similar radiation and air quality impacts.

To address some of these questions, we examine the June 2015 trans-Atlantic African dust storm, which is the second strongest aerosol extreme event over the tropical North Atlantic in boreal summer during 2003–2020 (Pu and Jin, 2021). We examine the characteristics, mechanism, and radiative and air quality impacts of this event using multiple satellite products (e.g., MODIS, VIIRS, CALIOP, CERES), ground observations (e.g., AERONET), and reanalysis data (ERA5). The following section reviews previous studies of summertime trans-Atlantic African dust events. Section 3 introduces the data and methodology used in this study, while section 4 presents a detailed analysis of the June 2015 event and compares it with the 2020 "Godzilla" dust event. Section 5 discusses limitations and uncertainties, and section 6 summarizes our major findings.

2 Background

During summertime, due to strong surface heating in the Sahara and dry convection (Fontaine et al., 2002), a deep, dry, well-mixed dust layer, i.e., the SAL, is formed over North Africa (Carlson and Prospero, 1972; Prospero et al., 2002; Barkan et al.,

2004; Braun, 2010; Pan et al., 2011; Dunion, 2011; Adams et al., 2012). The top layer of a SAL can reach 5-6 km while its base is often about 0.9-1.8 km above the surface (e.g., Prospero and Carlson 1972; Dunion and Velden 2004; Adams et al. 2012). Early observational studies documented that SALs often move westward from North Africa to Barbados in the Caribbean (Prospero and Carlson, 1970; Prospero et al., 1970). It is estimated that at least 72 Tg a^{-1} of African dust leaves the African west coast at 15°W in summer and about 18 Tg a^{-1} reaches 75°W in the Caribbean (Yu et al. 2015).

The westward transport of the SAL in boreal summer has long been related to meteorological factors, such as the African easterly jet (AEJ) and African easterly wave (AEW) (Burpee, 1972; Fontaine et al., 2002; Jones et al., 2003; Engelstaedter and Washington, 2007). In addition, many other factors that either influence dust emissions in North Africa or affect atmospheric circulation over the tropical North Atlantic have been related to the variations in the westward transport of African dust in summer, e.g., El Niño Southern Oscillation (ENSO) events (Prospero and Lamb, 2003; Li et al., 2021; Yin et al., 2022), Atlantic sea surface temperatures (Wang et al., 2012), and local vegetation coverage (Moulin and Chiapello, 2004; Yu et al., 2015a) that modulate dust emissions and near-surface dust concentrations (Prospero and Lamb, 2003; Li et al., 2021; Yin et al., 2022), the North Atlantic subtropical high (NASH; Doherty et al. 2008; Chen et al. 2018) and the North Atlantic Oscillation (NAO; Moulin et al. 1997) that affect the dust transport over the tropical North Atlantic.

While the above studies extensively examined the features and propagations of the SALs in summer, only a few studies focused on extreme trans-Atlantic dust African events that lead to high dust loading over the tropical North Atlantic and the Caribbean Basin. For instance, Petit et al. (2005) examined the extreme trans-Atlantic dust event in June 1994. The dust plume originated near the saltpan of Taoudenni in northern Mali (Fig. S1a), where strong surface winds and convection associated with a depression lifted dust to about 5 km. The dust plume then gradually descended as it traversed the Atlantic within the easterly trades to the eastern Caribbean Basin.

Huang et al. (2010) conducted a comprehensive study of major trans-Atlantic African dust outbreaks from 2003 to 2007. Dust outbreaks were defined when regionally averaged daily MODIS aerosol optical depth (AOD) exceeded the climatological mean by one standard deviation over the eastern tropical North Atlantic. Their findings painted a detailed picture of dust transport from central Western Africa to the Caribbean Basin, documenting the westward transport pathways of dust, the speed and altitude of dust layers, and their connection with dry air outbreaks. While Huang et al. (2010) are among the first to systemically study severe trans-Atlantic dust outbreaks, they did not examine the large-scale circulation conditions supporting long-range transport of African dust plumes, nor the local land surface conditions associated with dust emissions.

The formation of the recent extreme trans-Atlantic Saharan dust event in June 2020, i.e., the "Godzilla" dust event, has been related to both enhanced local emissions that are associated with increased surface winds, reduced vegetation coverage (Pu and Jin 2021), and strong haboobs (Yu et al. 2021) and large-scale circulations that favored the westward transport of African dust (Francis et al., 2020; Yu et al., 2021; Pu and Jin, 2021). Pu and Jin (2021) pointed out that atmospheric circulation extremes played important roles in this event. While the extremely enhanced AEJ advected huge amounts of dust to the eastern

tropical North Atlantic, the westward extension of the NASH and the greatly intensified Caribbean low-level jet (CLLJ) further steered the dust plume westward and northward to the U.S. Here we will examine whether similar atmospheric circulation patterns and land surface conditions occurred in the June 2015 event and if circulation extremes also contributed to the high dust loading over the Atlantic.

We will also examine the impacts of the extreme trans-Atlantic dust event in June 2015. Dust aerosols are known to absorb and scatter incoming shortwave and outgoing longwave radiation and also emit longwave radiation, affecting the regional and global radiative balance (Claquin et al., 2003; Xu et al., 2017). The sign and magnitude of the radiative forcing of dust strongly depend on the physical and optical properties of dust aerosols, their chemical and mineral compositions, and spatial distributions (Goudie and Middleton, 2001; Meloni et al., 2005; Reddy et al., 2013; Mahowald et al., 2014; Kok et al., 2023)The radiative effects of African dust have long been examined through satellite products (e.g., Yu et al. 2006; Brindley and Russell 2009; Song et al. 2018), field campaigns (e.g., Carlson and Caverly 1977; Haywood et al. 2001, 2003; Highwood et al. 2003; Slingo et al. 2006), and modelling studies (e.g., Tegen and Lacis 1996; Myhre et al. 2003; Tegen et al. 2010; Hansell et al. 2010). The high dust loading, long duration, and large affected areas of extreme trans-Atlantic dust events provide great examples to revisit the radiative impacts of African dust. Francis et al. (2022) found that the "Godzilla" dust plume in 2020 led to a 190 W m^{-2} drop in downward shortwave radiation flux and a 23 W m^{-2} rise in downward longwave flux at the surface of the eastern tropical Atlantic on 18 June 2020. Mehra et al. (2023) showed that the "Godzilla" dust plume also impacted radiative balance in the U.S., resulting in atmospheric heating of 5-12 W m^{-2}. Here we will explore the perturbation of the June 2015 African dust plume on both surface and TOA radiative budgets.

Severe dust storms with elevated concentrations of dust particles can have adverse impacts on public health and transportation (e.g., Shinn et al., 2003; Goudie, 2014; Española et al., 2021). Trans-Atlantic African dust is found to affect air quality over both the Caribbean Basin and the southern U.S. (Prospero, 1999; Chen et al., 2018; Prospero et al., 2021). For instance, Saharan dust is found to be related to high rates of asthma in the Caribbean (Gyan et al., 2005; Akpinar-Elci et al., 2015) and can transport fungi and bacteria from Africa to the Caribbean (Prospero et al., 2005; Waters et al., 2020). Over coastal Texas, African dust contributed approximately 8% of $PM_{2.5}$ (particulate matter with aerodynamic diameter < 2.5 μm) concentrations in summer, and up to 48% of $PM_{2.5}$ during an African dust outbreak in August 2014 (Bozlaker et al., 2019). During the "Godzilla" event in 2020, $PM_{2.5}$ levels over a large area of the southern U.S. exceeded the Environmental Protection Agency (EPA)'s guideline, and the Air Quality Index (AQI) reached orange (unhealthy for sensitive groups) and red (unhealthy for the general public) levels in more than 11 states (Pu and Jin, 2021; Yu et al., 2021). To what extent the 2015 extreme trans-Atlantic dust affected the air quality in the U.S. will be examined in this study.

3 Data and Methodology

3.1 Data

We use satellite retrievals of AOD, radiative fluxes, vegetation coverage, and precipitation, as well as circulation variables and soil moisture from reanalysis and ground observations of AOD and air quality variables to examine the characteristics, mechanisms, and impacts of the 2015 extreme dust plume.

3.1.1 MODIS and VIIRS AOD

AOD is a column-integrated measure of aerosol extinction. Here, daily and monthly AOD from the Moderate Resolution Imaging Spectroradiometer (MODIS) (version 6.1; Sayer et al. 2019) aboard both the Terra and Aqua satellites are used. Monthly level 3 AOD data from 2003 to 2022 have a spatial resolution of 1.0° × 1.0°, while daily level 2 data in 2015 are re-gridded to a 0.1° × 0.1° grid to characterize features of the dust plume. Monthly and daily MODIS AOD is generated by averaging Terra and Aqua MODIS AOD.

Daily AOD from the Visible Infrared Imaging Radiometer Suite (VIIRS, Hsu et al., 2019) on board the Suomi National Polar-Orbiting Partnership (Suomi-NPP) satellite is used to complement MODIS AOD. Daily VIIRS AOD is also gridded to a 0.1° × 0.1° resolution and averaged with MODIS AOD during June 2015 to increase data spatial coverage to better demonstrate the propagation of the African dust plume. Both MODIS and VIIRS AOD agree well with the Aerosol Robotic Network (AERONET; Holben et al. 1998, 2001) ground observations (Liu et al., 2014; Sayer et al., 2019; Hsu et al., 2019), with root mean square errors of 0.115, 0.121 and 0.122 for Aqua-MODIS, Terra-MODIS, and VIIRS, respectively (Hsu et al., 2019). The high spatial resolutions, near-global coverage, and relatively small errors in MODIS and VIIRS AOD make them very suitable for examining the long-range transport of extreme African dust plumes.

3.1.2 CALIOP Aerosol Profiles

The Cloud-Aerosol Lidar with Orthogonal Polarization (CALIOP) is a two-wavelength lidar instrument aboard the Cloud-Aerosol Lidar and Infrared Pathfinder Satellite Observations (CALIPSO) satellite. CALIOP measures backscattered radiances attenuated by aerosols and clouds and retrieves the microphysical and optical properties of aerosols. The record began in June 2006 and has been shown to provide quality data about aerosol size, type, and different shapes of cloud particles (Winker et al., 2007). We used daily 532 nm total attenuated backscatter (level 1) and depolarization ratio (δ; level 2) in June 2015 to examine the vertical profiles of the dust plume. Note that CALIOP data are missing from 19–28 June 2015. The instrumental sources of depolarization bias are small (Winker et al., 2004), with a typical (median values) uncertainty of about 0.18 for aerosol profile products at nighttime (CALIPSO user guide 2018), while the biases of nighttime attenuated backscatter at 532nm in version 4 are about 1.6%±2.4% when compared to collocated measurements from the Langley Research Center

airborne High Spectral Resolution Lidar (Kar et al., 2018). Since the depolarization ratio can help separate spherical and non-spherical hydrometeors (Sassen, 1991), we use $\delta \geq 0.2$ to separate dust (non-spherical) from other aerosols (Li et al., 2010; Kim et al., 2018; Pu and Ginoux, 2018a; Pu and Jin, 2021).

3.1.3 SEVIRI dust RGB

Dust red-green-blue (RGB) composite satellite images have been widely used as a qualitative method to study the spatiotemporal formation and evolution of dust plumes (e.g., Schepanski et al. 2007; Marsham et al. 2008; Martínez et al. 2009; Roberts et al. 2018; Caton Harrison et al. 2021). Dust aerosols are detected based on spectral varying emissivity at the infrared (IR) wavelengths ranging from 8 to 12 μm (Ackerman, 1997; Lensky and Rosenfeld, 2008). Here, the dust RGB images from the Spinning Enhanced Visible and Infrared Imager (SEVIRI) onboard the geostationary Meteosat Second Generation (MSG) satellite (Schmetz et al., 2002) positioned at 0° longitude (i.e., Meteosat-10) are used to understand dust emissions during the June 2015 extreme event. SEVIRI observes the Earth system at 12 wavelengths ranging from 0.4 to 13.4 μm with a 15-minute repeat cycle and a spatial resolution of 3 km at nadir for the IR channels. SEVIRI dust RGB images are composed of brightness temperatures (BT) and BT difference (BTD) at 8.7, 10.8, and 12.0 μm (Schepanski et al., 2007; Ashpole and Washington, 2012). The dust RGB bands are defined as follows: BTD of 12.0−10.8 μm is red, BTD of 10.8−8.7 μm is green, and BT at 10.8 μm is blue. The dust plumes appear as pink in the dust RGB images. IR dust detection is affected by several factors, such as the vertical temperature gradient in the lower atmosphere, water vapor content, dust mineralogy, dust altitudes, and characteristics of the land surface (Brindley et al., 2012; Banks et al., 2018, 2019). Here, the high temporal-resolution dust RGB images complement MODIS and VIIRS daily AOD to show the development of the dust plume over North Africa.

3.1.4 MODIS NDVI

We also use monthly and 16-day Terra MODIS Normalized Difference Vegetation Index (NDVI; Didan et al. 2015; version 6.1) to examine the connection between dust emissions and vegetation coverage. The level 3 data are interpolated to a 0.25° × 0.25° grid, and the 16-day products are linearly interpolated to daily values. The uncertainty of the data is about ±0.025 (MODIS GAS 2023), which is much smaller than the anomalies in the Sahel as noticed in the study.

3.1.5 IMERG

The Global Precipitation Measurement Mission (GPM) utilizes the Integrated Multi-Satellite Retrievals for GPM (IMERG) algorithm to combine all available low-Earth-orbit and geosynchronous-Earth-orbit satellite passive microwave (PMW) and infrared (IR) precipitation estimates and is then validated and bias-corrected with monthly gauge analysis from the Global Precipitation Climatology Centre (GPCC) (Huffman et al. 2018). IMERG is an improvement over the previous Tropical

Rainfall Measuring Mission (TRMM), with reduced miss-detection of precipitation and better performance in capturing heavy and light precipitation (Wang et al., 2021) and sub-daily rainfall (Freitas et al., 2020), but still has large overestimations of duration and underestimations of intensity of precipitation (Freitas et al., 2020). We use IMERG Final Run (IMERG-F) from 2000 to 2019 (0.1° by 0.1°) as it is the most accurate, gauge-adjusted, and research-ready IMERG product (Wang et al., 2017, 2021; Beck et al., 2021). The half-hourly data are resampled to daily averages to examine the potential influence of precipitation on the formation and transport of the extreme African dust plume.

3.1.6 CERES Radiative Fluxes

We use daily and monthly radiation flux data from the Clouds and the Earth's Radiant Energy System (CERES) products (Doelling et al., 2016) on a 1°×1° grid to study the radiative impacts of the extreme 2015 dust plume. The CERES instruments are onboard both the Terra and Aqua satellites, measuring shortwave (SW) radiation between 0.3 and 5 μm, total radiation between 0.3 and 200 μm, and window wavelengths between 8 and 12 μm (Wielicki et al., 1996). The dataset includes observed top of the atmosphere (TOA) fluxes and computed surface and in-atmosphere fluxes using Langley Fu-Liou radiative transfer model and MODIS and geostationary satellite-derived cloud properties, along with atmospheric data from GEOS-5.4.1 and aerosol prosperities from the Model for Atmospheric Transport and Chemistry (MATCH) that assimilates MODIS AOD (Rutan et al., 2015). Note that current CERES products have a net imbalance of +4.5 W m^{-2} at TOA (Johnson et al., 2016; Kato et al., 2018; Loeb et al., 2018). In comparison with surface observations on buoy sites, CERES surface fluxes show mean biases of 3.0 W m^{-2} for downward SW and -4.0 W m^{-2} for downward longwave (LW) fluxes in monthly data. The larger differences between the CERES and buoy data over the tropical Atlantic Ocean are attributed to the transported African dust that accumulated on buoys (Foltz et al., 2013). Due to its high spatial coverage, CERES products have been widely used to study the radiative effect of dust (e.g., Song et al. 2018; Francis et al. 2022).

3.1.7 AERONET AOD

The AERONET program (Holben et al., 1998) provides quality-assured cloud-screened (level 2.0) measurements of aerosol optical properties from sun photometer records. The recorded AOD has high accuracy with an uncertainty level of 0.01-0.02 (wavelength dependent) (Holben et al., 2001; Giles et al., 2019). Here version 3.0 AOD at wavelengths between 440 nm and 870 nm and Ångström exponents across the dual wavelength of 440–675, 440–870, and 500–870 nm with temporal resolutions varying from about 3 to 30 minutes (station dependent) over western North Africa, the tropical North Atlantic, and Caribbean Basin in June 2015 are used. AOD at 550 nm is converted using the method detailed by Pu et al. (2020). Stations with records less than 10 days and AOD mean values over 11–25 June 2015 lower than 0.2 are not included in the analysis. The results of 14 stations are presented and compared with MODIS and VIIRS AOD.

3.1.8 EPA Station Data

Daily air quality data of $PM_{2.5}$ and the Air Quality Index (AQI) from the U.S. Environmental Protection Agency's (EPA) Air Quality System (AQS) stations are used to examine the influence of the June 2015 African dust plume on air quality in the U.S. AQI reflects the health effect of major air pollutants, with values of 0–50 indicate good air quality (symbolized by green), 51–100 for moderate condition (yellow), 101–150 for unhealthy for sensitive groups (orange), and 151–200 for unhealthy condition (red).

3.1.9 MERRA-2 Aerosol Products

The Modern-Era Retrospective Analysis for Research and Applications, Version 2 (MERRA-2; Gelaro et al. 2017) provides dust optical depth (DOD) (50 km; 3-hourly) beginning in 1980. MERRA-2 is the first long-term global reanalysis that incorporates satellite observations of aerosols (Gelaro et al., 2017). MERRA-2 assimilates aerosol products from MODIS, Multi-angle Imaging SpectroRadiometer (MISR), and Advanced Very-High-Resolution Radiometer (AVHRR) as well as ground observations from AERONET sun photometers (Gelaro et al., 2017; Buchard et al., 2017). MERRA-2 shows considerable skill in its aerosol products and improvement over its predecessor (Gelaro et al., 2017; Randles et al., 2017; Buchard et al., 2017). Its DOD product well captures the spatial and temporal variations in DOD over North Africa on the seasonal time scale in comparison with infrared satellite retrievals but misses a large part of day-night differences of dust as night-time observations currently are not assimilated to the product (Tindan et al., 2023). The 3-hourly MERRA2- DOD are averaged to daily data to complement MODIS and VIIRS AOD.

3.1.10 ERA5 Meteorological and Surface Variables

European Centre for Medium-range Weather Forecasts (ECMWF) Reanalysis 5 (ERA5) (Hersbach et al., 2020; Muñoz-Sabater et al., 2021) is the fifth generation of the ECMWF reanalysis products. Monthly and hourly variables such as surface winds and winds and geopotential height at 925, 850, and 600 hPa on a resolution of 0.25° × 0.25° are used to understand circulation features associated with dust emissions and long-range transport.

Hourly and monthly volumetric soil water of the top layer (i.e., 0–7cm) with a spatial resolution of 0.1° × 0.1° is used to examine land surface conditions associated with dust emissions. Daily values are averaged from hourly data. ERA5 is the first ECMWF reanalysis to incorporate soil moisture retrievals from C-band scatterometer instruments onboard European Remote Sensing satellites-1,2 (ERS-1, 2) and Meteorological Operational satellites A, B (MetOp-A, B) (Piles et al., 2019; Hersbach et al., 2020; Agutu et al., 2021; Muñoz-Sabater et al., 2021). Although its soil moisture product does not incorporate ground-based observations and lacks sufficient spin-up time to accurately represent deep soil moisture, ERA5 soil moisture estimates show high skill for shallow soil moisture in regions where gauge measurements are lacking, such as western Africa (Brocca et al., 2020; Beck et al., 2021; Muñoz-Sabater et al., 2021).

3.2 Jet Indices

Both the African easterly jet (AEJ) and the Caribbean low-level jet (CLLJ) are found to affect the westward propagation of African dust plumes (Prospero and Carlson, 1981; Pu and Jin, 2021). The extremely enhanced easterly jets also contributed to the development of the "Godzilla" dust event in June 2020 (Pu and Jin 2021). Here we examine how these jets may affect the formation of the extreme African dust plume in 2015. We use jet indices to quantify the magnitude of the jets, which are calculated by averaging easterly wind speed over their climatological locations, similar to regions selected in prior papers (Cook, 1999; Wang, 2007; Leroux and Hall, 2009; Martin and Schumacher, 2011). Following Pu and Jin (2021), the CLLJ index is calculated by averaging ERA5 925 hPa easterly wind between 11°N – 17°N and 70°W – 80°W, and the AEJ index is calculated by averaging ERA5 600 hPa easterly wind speed between 10°N – 15°N and 30°E – 10°W.

3.3 Identify Extreme Trans-Atlantic Dust Events

We first use aerosol extreme events (AEE; Pu and Jin 2021) to identify high dust loading days over the tropical North Atlantic and western North Africa. An AEE is defined when the regional mean daily MODIS AOD is above the 90^{th} percentile of daily AOD centered on a 15-day window during 2003–2022 in boreal summer (June–August). The duration of an AEE is defined as the number of consecutive days (≥1) that meet the criteria, while the magnitude of an AEE is calculated by averaging AOD during the event. Following Pu and Jin (2021), we calculated AEEs over the tropical North Atlantic (8°N – 25°N, 18°W – 90°W; see location in Figure 1a) and over the western North Africa dust source region (8°N – 25°N, 18°W – 5°W; see Figure 1a) for JJA 2003–2022. During boreal summer peak dust activities are mainly located in western North Africa, extending from the Mauritanian coast to the Mali–Mauritania border and Mali–Algeria border (Goudie and Middleton, 2001; Prospero et al., 2002; Engelstaedter et al., 2006; Engelstaedter and Washington, 2007). The averaging regions largely capture the westward transport pathway of African dust in summer, and the resultant AEEs over 2003-2022 are very similar to those of by Pu and Jin (2021; their Fig. 2). Over the tropical North Atlantic region, the AEE in June 2020 has the highest magnitude of AOD in the record, with a duration of 12 days (not shown), and the June 2015 event is the second highest, with a duration of six days (Figure 1c). Over the dust source region in western North Africa, a one-day AEE event on June 13 is found, with a moderately high AOD of 0.74 (Fig. 1b), weaker than that in June 2020 (a six-day AEE of 0.90) and slightly above the mean of AEEs over western North Africa (0.73; Fig. 1d). Note MODIS AOD in the study region contains missing values largely due to cloud screening which may affect the calculation of AEEs. Here, only days where the averaging area has less than 30% missing AOD values are used in AEE calculations, and this criterion mainly affects the AEEs over land (Fig. 1b). Slightly increasing or reducing the missing value threshold (e.g., to 20% or 40%) does not change the AEE days over the ocean.

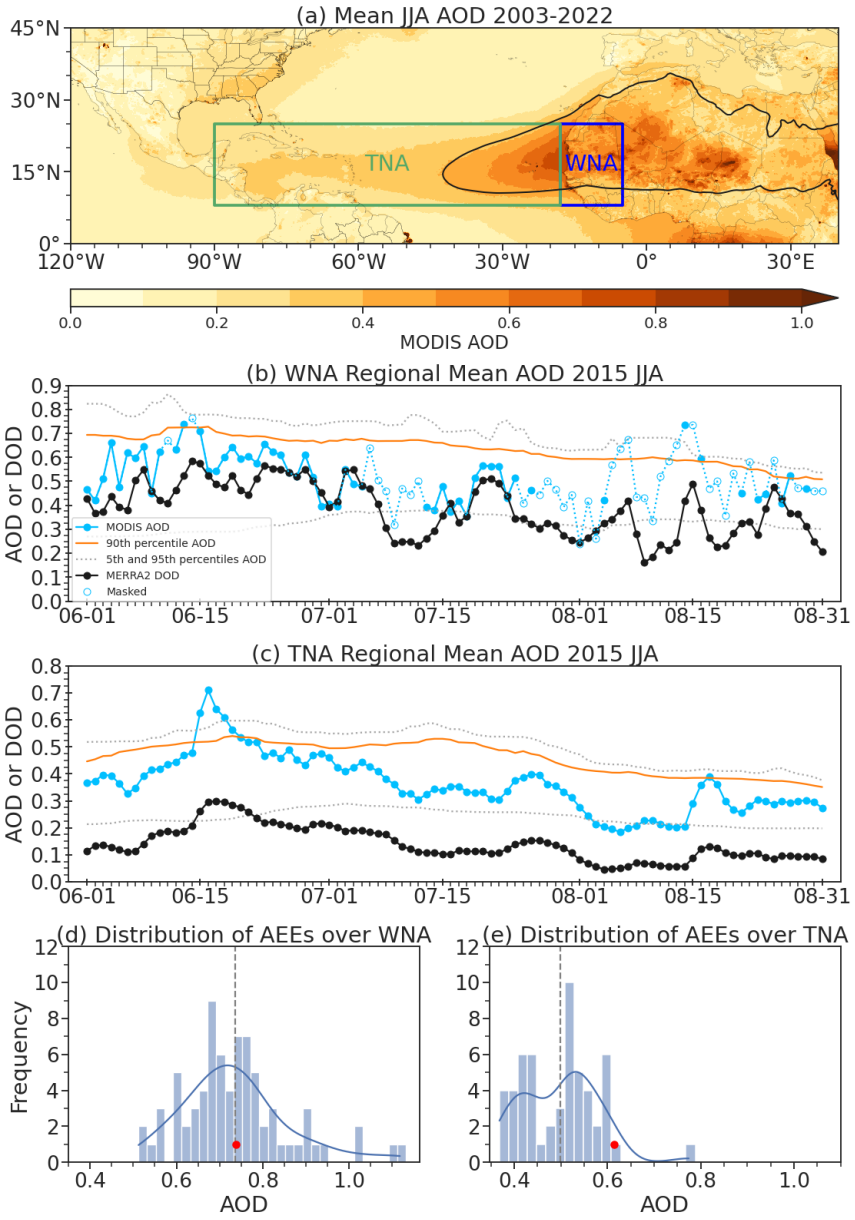

Figure 1. (a) Climatology of MODIS AOD in JJA from 2003 to 2022. Regions with MERRA-2 DOD ≥ 0.3 are contoured in black. The averaging area over the tropical North Atlantic (TNA; 8°N - 25°N, 18°W - 90°W) and western North Africa (WNA; 8°N - 25°N, 18°W - 5°W) regions are marked by green and blue boxes, respectively. Regional mean daily MODIS AOD (blue) and MERRA-2 DOD (black) in JJA 2015 over (b) western North Africa and (c) the tropical North Atlantic. The 90th percentile of daily MODIS AOD in JJA (2003–2022) is shown in orange and the grey dotted lines represent the 5th and 95th percentiles of AOD. Filled (empty) circles represent days with less than (more than) 30% missing values within the regional boxes. Distribution of AEEs from 2003-2022 over (d) WNA, and (e) TNA. Red dots mark values of the June 2015 event, and the vertical dashed lines denote means of AEEs over WNA and TNA.

While AEEs capture the maxima AOD during the event (Figures 1b-c), a trans-Atlantic event usually lasts more than a week as it takes about seven days for African dust to reach the Caribbean and 10–12 days to reach the continental U.S. (Ott et al.,

1991; Haarig et al., 2017; Chen et al., 2018). Thus, we also use an AOD Hovmöller diagram over the tropical North Atlantic that shows the westward propagation of dust plume (Figure 2) and a daily AOD plot (Figure 3) to identify the beginning and ending dates of the event. We found that the extreme dust event started around 12 June and ended around 23 June 2015.

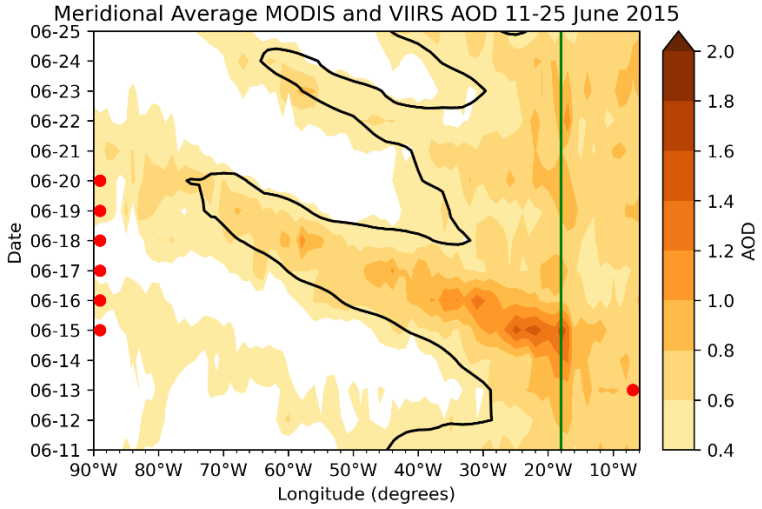

Figure 2. Hovmöller plot of the meridional averaged MODIS and VIIRS AOD from 8°N - 25°N across the tropical North Atlantic from 11 June to 15 June 2015. Only AOD above 0.4 is shown. The black contour denotes the areas where MERRA-2 DOD ≥ 0.3. The green line denotes 18°W, the dividing line between the averaging boxes shown in Figure 1. Red dots mark the dates of AEEs over the tropical North Atlantic (left) and over western North Africa (right).

4 Results

4.1 Features of the extreme trans-Atlantic dust event in June 2015

Figure 3 shows the daily mean AOD averaged between MODIS and VIIRS from 11 to 25 June 2015. The extreme dust event began around 12 June, and on 12-13 June AOD reached the 95th percentile over the western Guinea coast. On the 14th AOD exceeded 2.0 over the borders of Mauritania, Mali, and Senegal (Figs. 3b-d). The plume was then rapidly advected out of the source region and into the tropical North Atlantic on 15 June. AOD over the west coast and tropical North Atlantic reached 4.95 (Fig. 3e). During its westward transport, large portions of the plume show AOD above the 95th percentile value in JJA over 2003–2022 and above the 99th percentile in some regions over the tropical North Atlantic (Figure S2). The dust plume arrived at the Caribbean Sea around 17 June (Fig. 3g) and passed through the region and began to split around 21 June (Fig. 3k). The northern branch of the plume was advected northward and dispersed across the Gulf region and the southern central and eastern U.S., while the southern branch of the plume travelled across the Guatemala Basin to the eastern tropical Pacific Ocean (Figs. 3l-o). The plume was still quite strong even after it passed into the Pacific, with daily AOD above the 99th percentile (Figs. S2m-o). Previous studies found that the westward movement of African dust in summer can reach 100 °W

(e.g., Vuolo et al. 2009; Adams et al. 2012). In this extreme event, the African dust plume travelled as far as 120 °W and beyond (Figs. 3l-o).

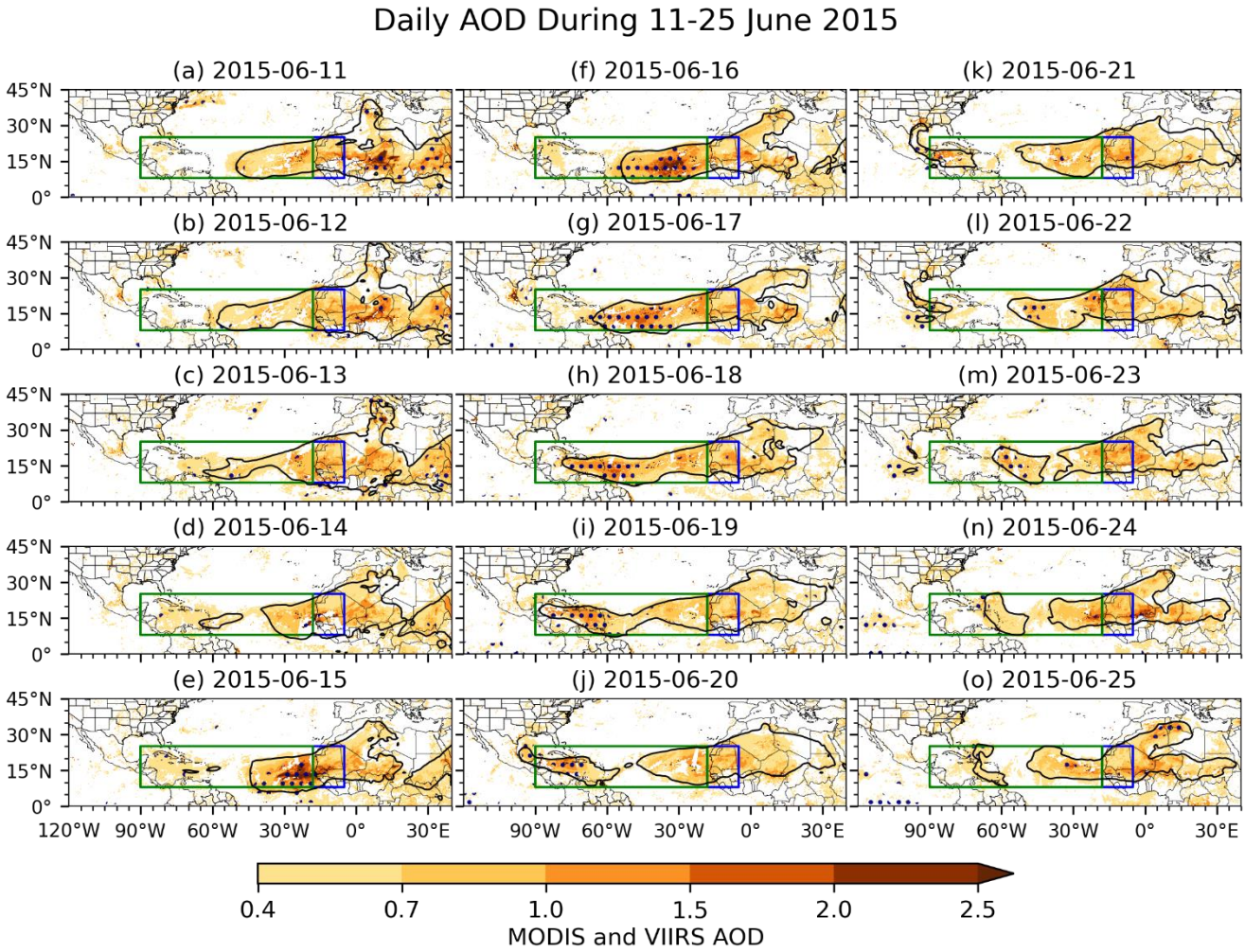

Figure 3. Combined MODIS and VIIRS AOD from 11 to 25 June 2015. Only AOD above 0.4 is shown. Black contours denote the boundary where MERRA-2 DOD ≥ 0.3. Navy dots represent regions where MODIS AOD is ≥ 95th percentile (with reference to daily MODIS AOD in JJA from 2003 to 2022 at each grid point). The green and blue boxes correspond to the averaging areas over the tropical North Atlantic and western North Africa, respectively.

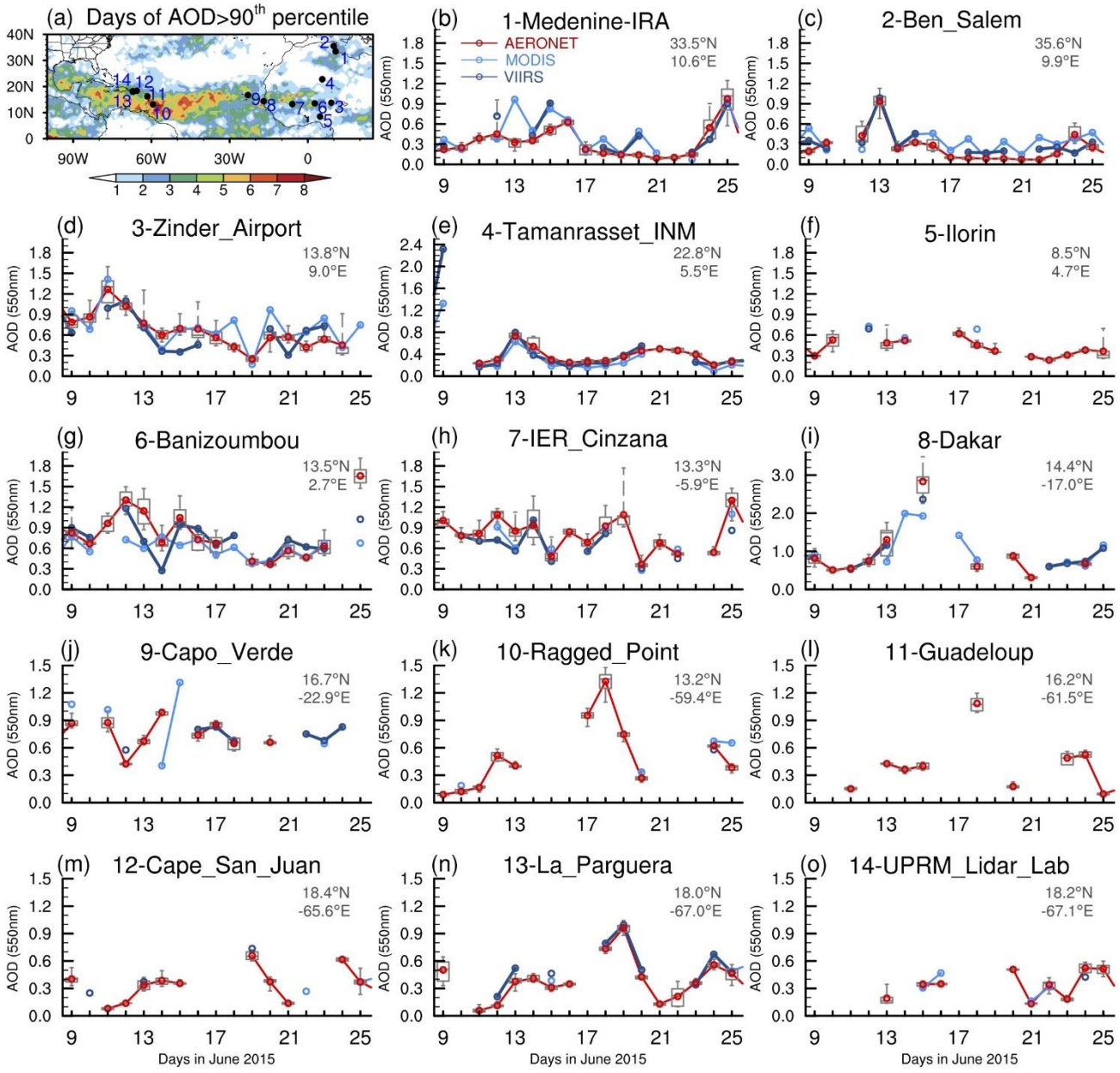

315

Figure 4. (a) Number of days when daily MODIS AOD greater than the 90th percentile of JJA daily values (2003–2022) during 12–24 June 2015. Locations of 14 AERONET stations are shown in black. (b)–(o) Daily AOD from AERONET (red), MODIS (light blue), and VIIRS (deep blue) during 9–25 June 2015. Sub-daily values of AERONET AOD are shown in the box in grey, with the upper, lower, and middle bars showing the 25th and 75th percentiles and median of the data and whiskers extending from the
320 **minimum to the maximum. The red circles denote the daily mean of AERONET AOD. The latitudes and longitudes of AERONET sites are shown on the top right.**

Figure 4a shows the number of days during this event with MODIS AOD greater than the 90th percentile of JJA daily values over 2003–2022 and the location of AERONET stations. Over the tropical North Atlantic, large areas experienced extremely high dust loading for two to six days. The evolution of AERONET AOD records (Figure 4b-o) largely resembles satellite AOD (Fig. 3). For sites over North Africa, AOD values slightly enhanced before or around 13 June 2015, with magnitudes largely less than 1.6, which is consistent with the findings in Fig. 1 that dust emissions over land were enhanced but not extremely high. Over the coastal region, the daily maximum AOD at Dakar reached 3.5 on 15 June (Fig. 4i) as the dust plume propagated toward the ocean (Fig. 2e). MODIS and VIIRS AOD showed a similar peak around 15 June at Dakar and Capo Verde sites, but in a weaker magnitude (Figs. 4i-j). When the dust plume reached the Caribbean Basin, AERONET AOD increased to 1.5 at the Ragged Point site on 18 June and 1.0 at the La Parguera site on 19 June. In comparison to AERONET records during the "Godzilla" event (Yu et al. 2021), daily mean AOD values were about 0.7 lower over the African coastal region and eastern tropical Atlantic (Dakar vs. Capo Verde) and about 0.3-0.8 lower over the Caribbean Basin at Ragged Point, Guadeloupe, and La Parguera sites.

CALIOP total attenuated backscatter shows the vertical profiles of dust plume (Figure 5). The plume was more compact and had a greater vertical extent (from 1.5 to 6 km) at its origin over western North Africa during 13-14 June 2015 (e.g., in between sampling points B and C in Fig. 5a-b). The high plume top over the source region is consistent with a previous study by Petit et al. (2005) who suggested that a minimum dust layer altitude of 3 km off the west coast of North Africa is necessary for African dust plumes to completely cross the Atlantic and enter the Caribbean, as dust plumes descend during westward transport. This descent is a balance between the convection in the underlying marine layer and the subsidence of anticyclonic air of the NASH (Petit et al., 2005). As the plume travelled westward over the tropical North Atlantic, it slowly subsided and weakened, consistent with previous studies (Braun, 2010; Adams et al., 2012; Groß et al., 2015; Weinzierl et al., 2017), although the rate of descent was somewhat slower than 500 m day^{-1} during the June 2020 event (Yu et al. 2021). By 18 June the plume over the western tropical North Atlantic was primarily between 2 and 5 km (Fig. 5f). Because CALIOP data were missing between 19 June and 28 June 2015, it is not entirely clear whether the descending rate increased as the plume propagated across the Caribbean Basin.

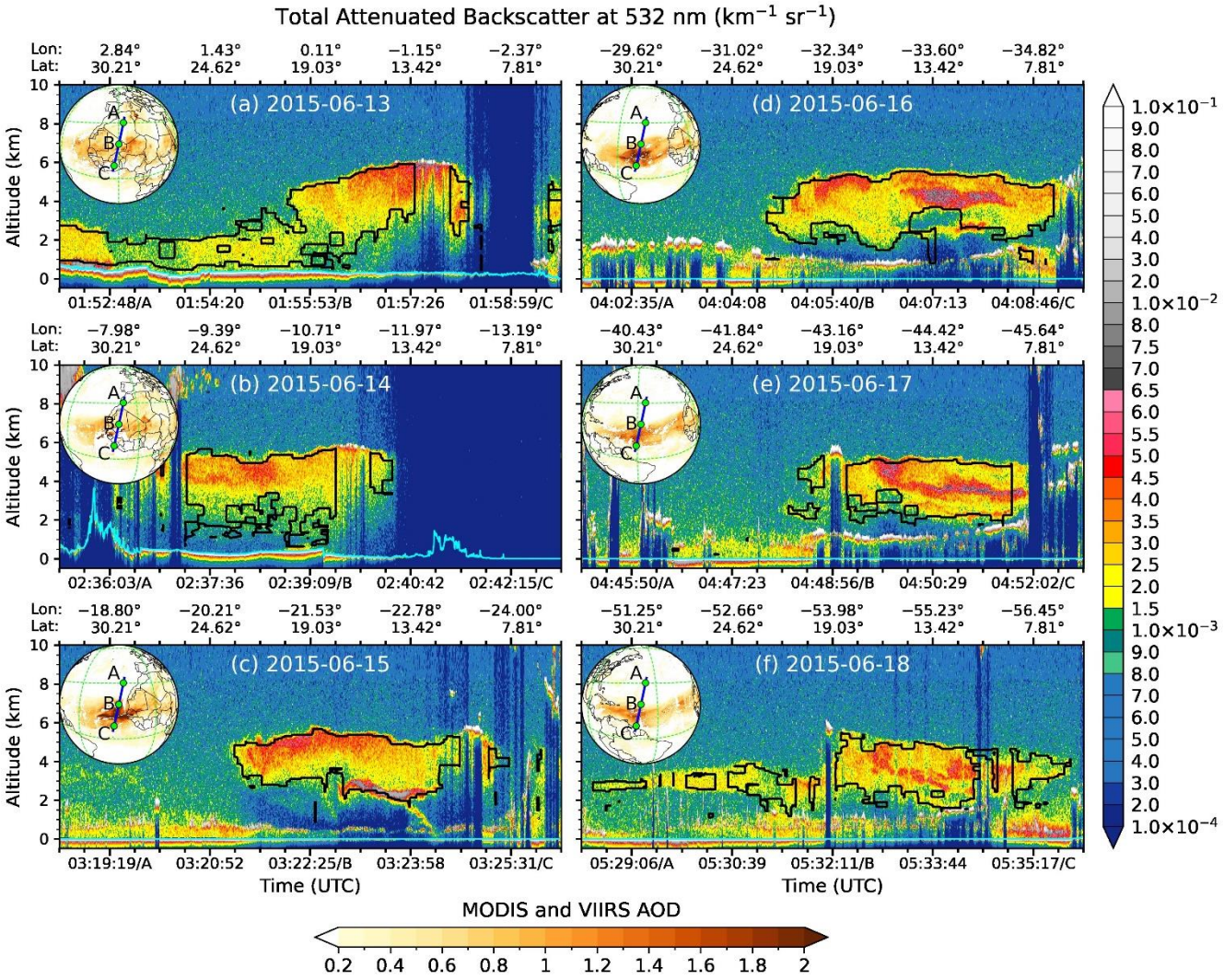

Figure 5. CALIOP 532 nm total attenuated backscatter (km^{-1} sr^{-1}) for 13–18 June 2015. The satellite tracks (blue lines) are displayed in the inset at the upper left of each panel with sampling points (A–C) corresponding to the x-axis of the cross-section and brown shading showing MODIS-VIIRS averaged AOD. Black contours denote dust aerosols (depolarization ratio ≥ 0.2). Surface elevation is indicated by cyan lines.

4.2 Circulation conditions associated with the 2015 extreme dust event

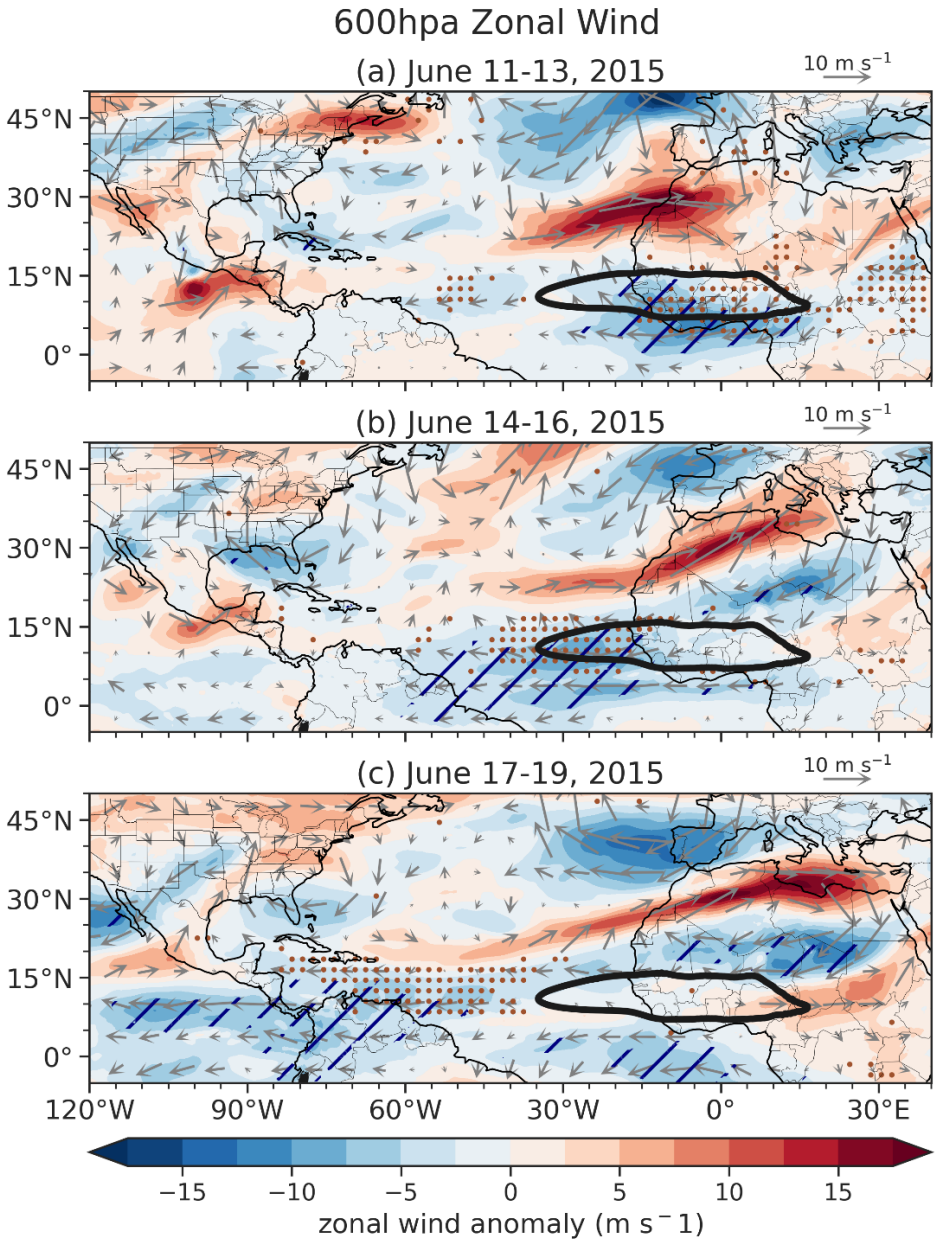

Figure 6. Anomalies of three-day mean 600 hPa winds (vectors; m s^{-1}) and zonal wind speed (shading; m s^{-1}) from 11 to 19 June 2015 with reference to the 1979–2022 climatology in June. Black contours show the climatological location of the African easterly jet (AEJ; denoted by zonal wind speed of -11 m s^{-1}). Hatches represent regions where easterly wind speeds ≥ 95th percentile (with reference to the absolute magnitude of three-day mean zonal wind speed in June from 1979 to 2022 at each grid point). Dots represent regions where MODIS AOD ≥ 95th percentile (with reference to daily AOD in JJA from 2003 to 2022 at each grid point) and ≥ 0.6.

In this section, we will examine the large-scale circulation patterns associated with the westward transport of the extreme African dust plume. Over western North Africa and the eastern North Atlantic, the AEJ centered around 600 hPa plays an important role in transporting African dust westward (Prospero and Carlson, 1981; Jones et al., 2003; Schepanski et al., 2017; Yu et al., 2021), with a stronger jet associated with higher AOD over the tropical North Atlantic (Pu and Jin 2021). Figure 6 shows anomalies of three-day averages of zonal wind speed at 600 hPa around the onset of the event (11–13 June 2015) to the time when the dust plume reached the Caribbean Basin (17–19 June 2015). The black contour shows the climatological location of the jet, and the hatched area denotes regions where zonal wind speed is above the 95th percentile in June during 1979–2022 in the ERA5 reanalysis. During 11–13 June, the easterly wind anomalies were located between 0°N and 17°N over the jet core region and the Guinea coast. The jet continued to intensify during 14–19 June, advecting the dust plume westward to the central tropical North Atlantic (Figs. 6b-c). The magnitude of the AEJ right before and at the beginning of the event (11–16 June) was 16.8 m s^{-1}, which is the fourth strongest for this week from 1979 to 2022 (Fig. S3a), greatly favoring the export and westward transport of African dust.

When the dust plume propagated to the central to western tropical North Atlantic, the anticyclonic flow of the NASH can further transport it westward. Figure 7a-c shows three-day averages of the geopotential height and wind anomalies at 850 hPa. The NASH had a westward extension from its climatological location toward the Gulf of Mexico and the southeastern U.S. from 17 to 25 June 2015. The related easterly and southerly wind anomalies further steered the dust plume toward the continental U.S. The westward extension of the NASH along with the reduced height over the tropical eastern Pacific further increased the meridional pressure gradient over the Caribbean Basin and strengthened the CLLJ at 925 hPa (Figs. 7d-f). In fact, the magnitude of the CLLJ during 17–22 June (18.3 m s^{-1}) is the strongest for the same period from 1979 to 2022 in the ERA5 reanalysis (Fig. S3b). Such a high magnitude of the jet is consistent with the extremely enhanced geopotential heights to the north of the Caribbean Basin and reduced heights to the south (hatched regions in Figs. 7a-c). The greatly strengthened CLLJ facilitated the westward transport of the African dust across the Caribbean Basin. The extreme easterly jet further advected part of the plume into the eastern Pacific, while the remainder of the plume was carried northward to the U.S. by the anticyclonic flow (Figs. 7e-f).

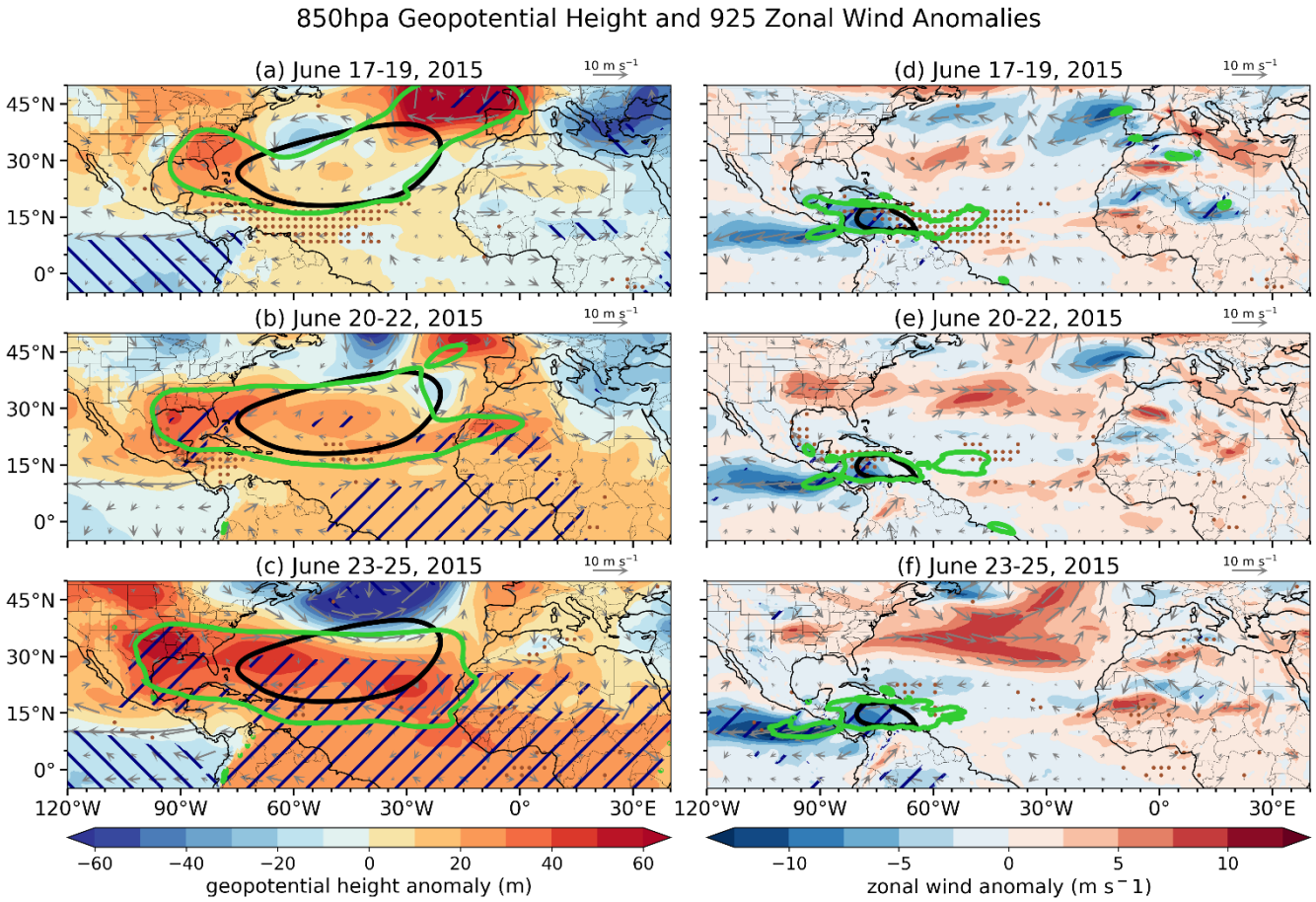

Figure 7. (a)-(c) Anomalies of three-day mean 850 hPa geopotential height (shading; gpm) and winds (vectors; m s^{-1}) with reference to the 1979-2022 climatology in June. Black contours show the climatological location of the North Atlantic subtropical high (NASH; (denoted by the 1560 gpm contour following Li et al. 2011), and green contours mark the three-day mean location of the NASH. Hatchings represent the top (≥ 95th; backward) and bottom (≤ 5th; forward) percentiles of geopotential height (with reference to June three-day mean values from 1979-2022 at each grid point). (d)-(f) Anomalies of three-day mean 925 hPa winds (vector; m s^{-1}) and zonal wind speed (shading; m s^{-1}) with reference to the 1979-2022 climatology in June. Black contours show the climatological location of the Caribbean low-level jet (CLLJ; denoted by the zonal wind speed contour of -11 m s^{-1}), and green contours mark the three-day mean location of the CLLJ. Hatchings represent regions where easterly wind speed ≥ 95th percentile (with reference to the absolute magnitude of three-day zonal wind in June from 1979-2022 at each grid point). In all panels, dots represent MODIS AOD ≥ 95th percentile (with reference to three-day mean AOD in JJA from 2003 to 2022 at each grid point) and ≥ 0.6.

Overall, the circulation patterns in the June 2015 event are largely consistent with the findings of Pu and Jin (2021), who showed that the enhanced AEJ and CLLJ and the westward extension of the NASH all contribute to the long-range transport of African dust to the tropical North Atlantic and the Caribbean Basin. The extremely high magnitudes of the AEJ and CLLJ in this event also suggest that circulation extremes played important roles in the formation of high dust loading over the ocean. One unique feature of the June 2015 event is the extremely strong CLLJ that transported a portion of the dust plume to the eastern Pacific, so fewer dust particles were being advected to the U.S.

4.3 Anomalous dust emissions

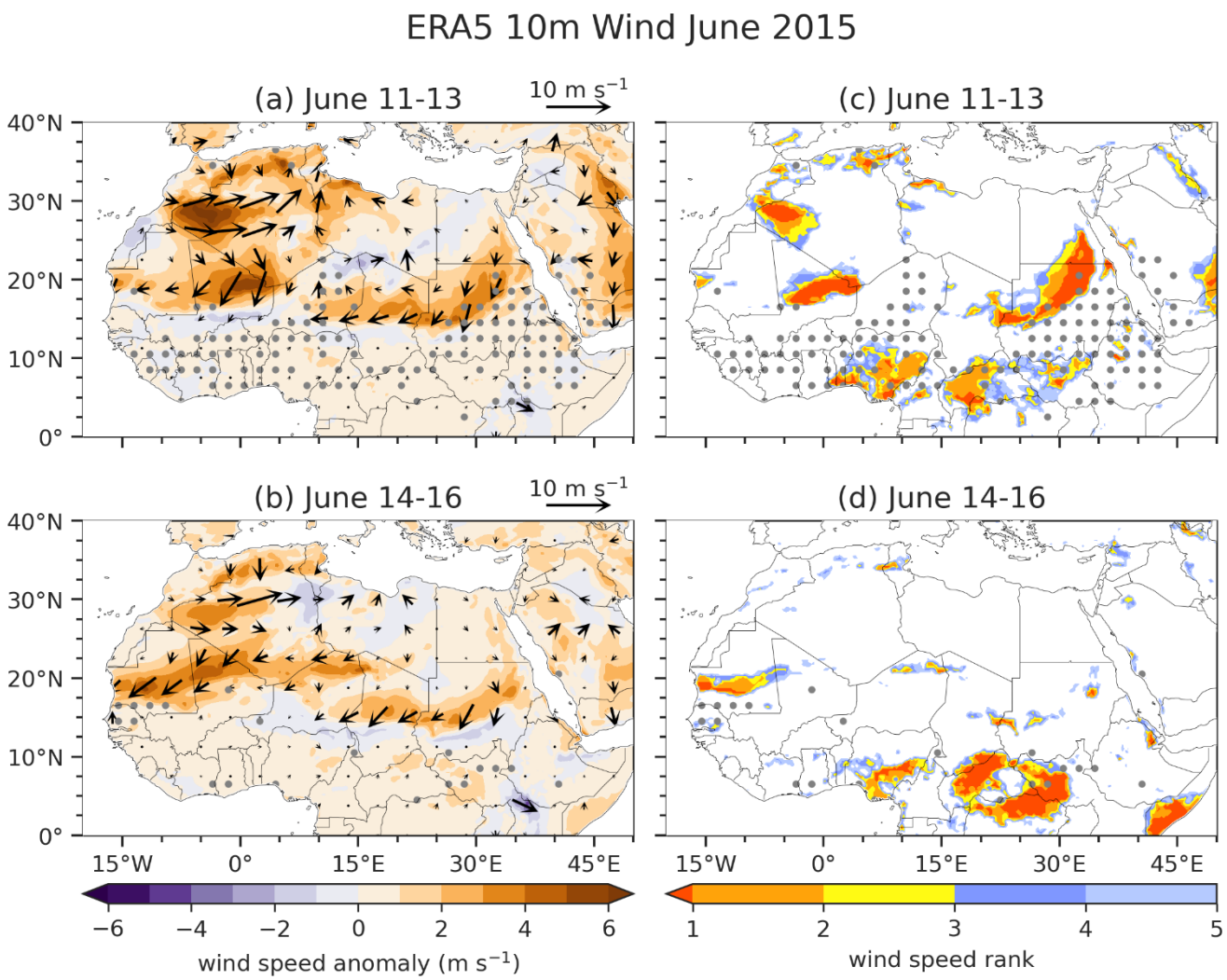

Figure 8. (a)-(b) Anomalies of 10 m winds (vectors; m s^{-1}) and wind speeds (shading; m s^{-1}) averaged over 11–13 June, and 14–16 June 2015 (with reference to the 1979-2022 climatology in June). (c)-(d) Ranking of daily surface wind speed averaged over 11–13 June and 14–16 June 2015, with reference to the corresponding three-day averages over 1979–2022 (44 years). Only wind speed rank 1– 5 (i.e., top five strongest) are shown. Areas with MODIS AOD ≥ 95th percentile (with reference to three-day mean AOD in JJA from 2003 to 2022 at each grid point) and ≥ 0.6 are dotted in grey.

As shown in Fig. 1b, the extreme trans-Atlantic dust event is associated with a one-day AEE on 13 June over western North Africa, which indicated enhanced dust emissions over source regions at the beginning of the event. To understand the factors that increased dust emissions we first examine local surface wind speed, which has long been related to dust emissions in North Africa (e.g., Gillette et al. 1980; Helgren and Prospero 1987; Engelstaedter and Washington 2007; Cowie et al. 2015; Evan et al. 2016). Figure 8 shows three-day averages of 10m surface wind anomalies from 11–16 June 2015 and the rank of

the top five strongest surface wind speeds during the same days from 1979–2022 over North Africa. Surface wind speeds are greatly intensified over eastern Mali to Mali-Algeria border, western Algeria, and southern Egypt to north Sudan (Figs. 8a-b; Fig. S1a). The magnitude of the surface wind speed ranked the highest or among the top five over summertime active dust source regions in central to eastern Mali (Fig. 8c) and Mauritania (Fig. 8d). High percentile AOD (grey dots) is largely located downstream of regions of extreme surface winds.

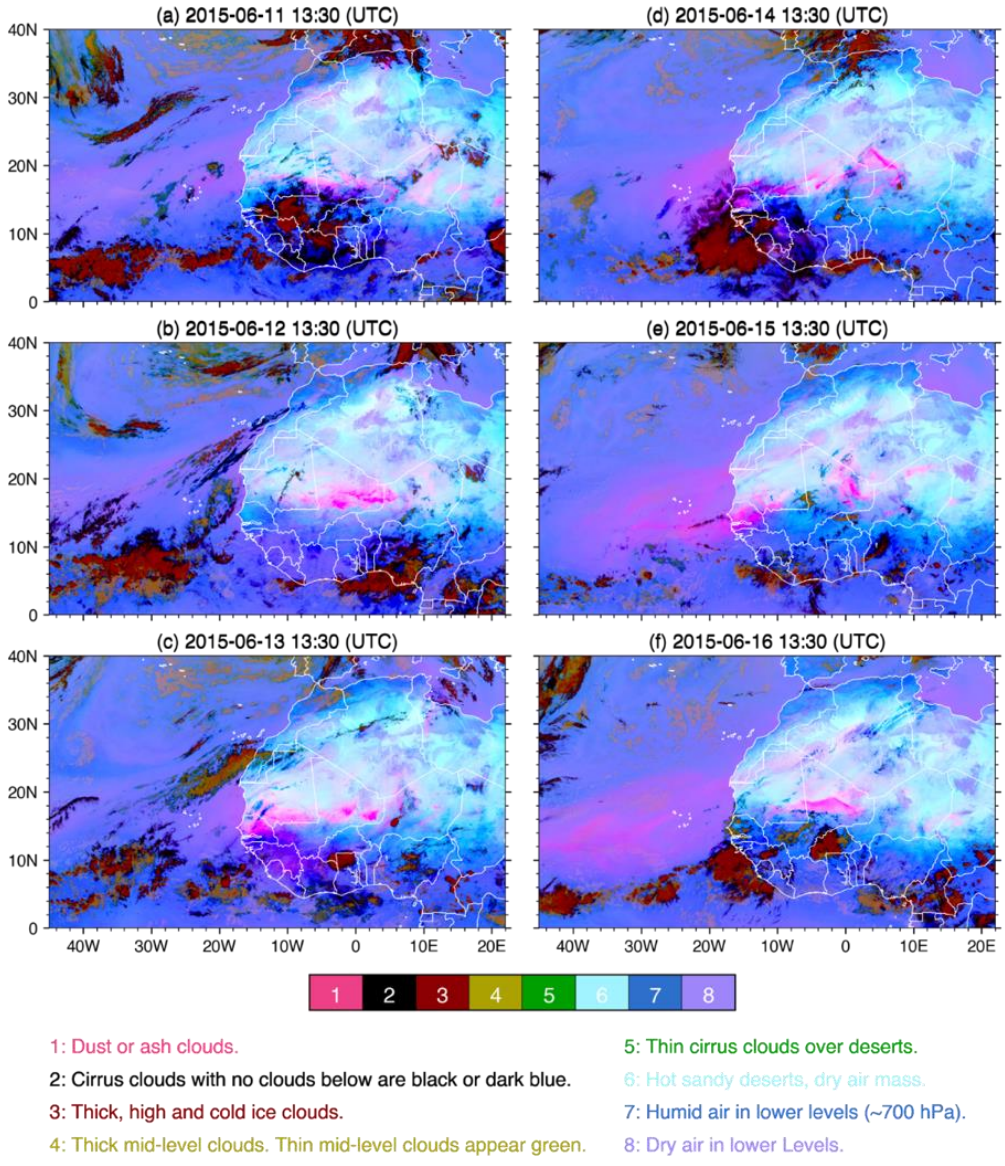

Figure 9. (a)-(f) Dust RGB from SEVIRI at 13:30 UTC from 11 to 16 June 2015. Dust plumes are denoted by pink shading (color 1), while deep convection is shown in dark red (color 3). Cirrus clouds, mid-level clouds, thin cirrus, hot sandy desert, low-level humid air, and low-level dry air are shown in black, dark golden, green, light cyan, blue, and purple, respectively.

The anomalously strong surface wind-induced dust emissions are also captured by the SEVIRI dust RGB images (Figure 9). While the dust emissions in Mali (pink) on 11 June 2015 were likely affected by the outflow of downdrafts generated by the mesoscale convective systems (MCSs) over southern to central Mali and Burkina Faso (dark red; Fig. 9a), the enhanced dust emissions over central Mali, Mali-Algeria-Niger border, and Mauritania during 12-16 June (Figs. 9 b-f) are largely collocated with the strong surface anomalies (Fig. 8c, d). On 14 June, a coastal MCS also contributed to the enhancement of dust emissions in Mauritania (Fig. 9d).

In addition to increased surface wind speeds, land surface conditions such as dry soil due to precipitation deficit and reduced vegetation coverage also favor dust emissions (Gillette et al., 1980; Engelstaedter et al., 2006; Cowie et al., 2014; Kim et al., 2017; Pu and Ginoux, 2018b). Figure 10 shows three-day averages of soil moisture anomalies from ERA-5 and NDVI anomalies from MODIS across North Africa. Soil moisture decreased over large areas in the Sahara and Sahel. In the southern Sahel soil moisture anomaly reached –0.1 m^3 m^{-3} (about –40%), below the 5th percentile during June 2003-2022 (Fig. 10a-b), likely as a result of decreased rainfall (Fig. S4). Note that the precipitation reduction over the tropical North Atlantic (Fig. S4) also helped maintain the high dust loading over the ocean by minimizing the scavenging of fine dust aerosols over the southern part of the dust plume around 5–10°N. Vegetation decayed almost over the same areas where soil moisture was greatly reduced, reaching the lower 5th percentile (Fig. 10c-d), even the lowest 1st percentile in some areas (not shown), favoring wind erosion in the region.

A multiple linear regression model has been used to quantify the relative contributions of land surface variables (i.e., surface wind speed, precipitation, and NDVI) to dust emissions over western North Africa in the "Godzilla" dust event in June 2020 (Pu and Jin 2021). Here we tested the same approach but using monthly surface wind speeds and top-layer soil moisture from the ERA5 and NDVI from MODIS as explanatory variables. Similar to the findings of Pu and Jin (2021), these variables can capture 64% of the variations of June AOD over western North Africa during 2003–2022 and largely reproduce the spatial pattern of AOD anomalies in the 2020 event (pattern correlation 0.86), although AOD magnitude is underestimated. However, we found that the statistical model cannot well reproduce the AOD anomalies in the June 2015 event (pattern correlation 0.21). A few factors may contribute to this discrepancy. The much shorter duration (i.e., one day) and weaker magnitude of the dust extreme over western North Africa during the 2015 event may be harder to capture in comparison with the stronger aerosol extreme that lasted six days in the 2020 event. Mechanisms that affect dust emissions on shorter time scales (e.g., from sub-hourly to daily) and smaller spatial scales (e.g., gusts generated by downdrafts from mesoscale convective storms) are not included in the multiple linear regression model. Non-linear interactions and feedback among explanatory variables are also not included. In addition, biases in explanatory variables, e.g., surface winds in North Africa are often underestimated in reanalyses (Largeron et al., 2015), could also affect the results. To fully quantify the contribution of each influencing factor on the formation of the trans-Atlantic dust event would require modelling studies with sensitivity tests, which is beyond the scope of this study and will be examined in the future.

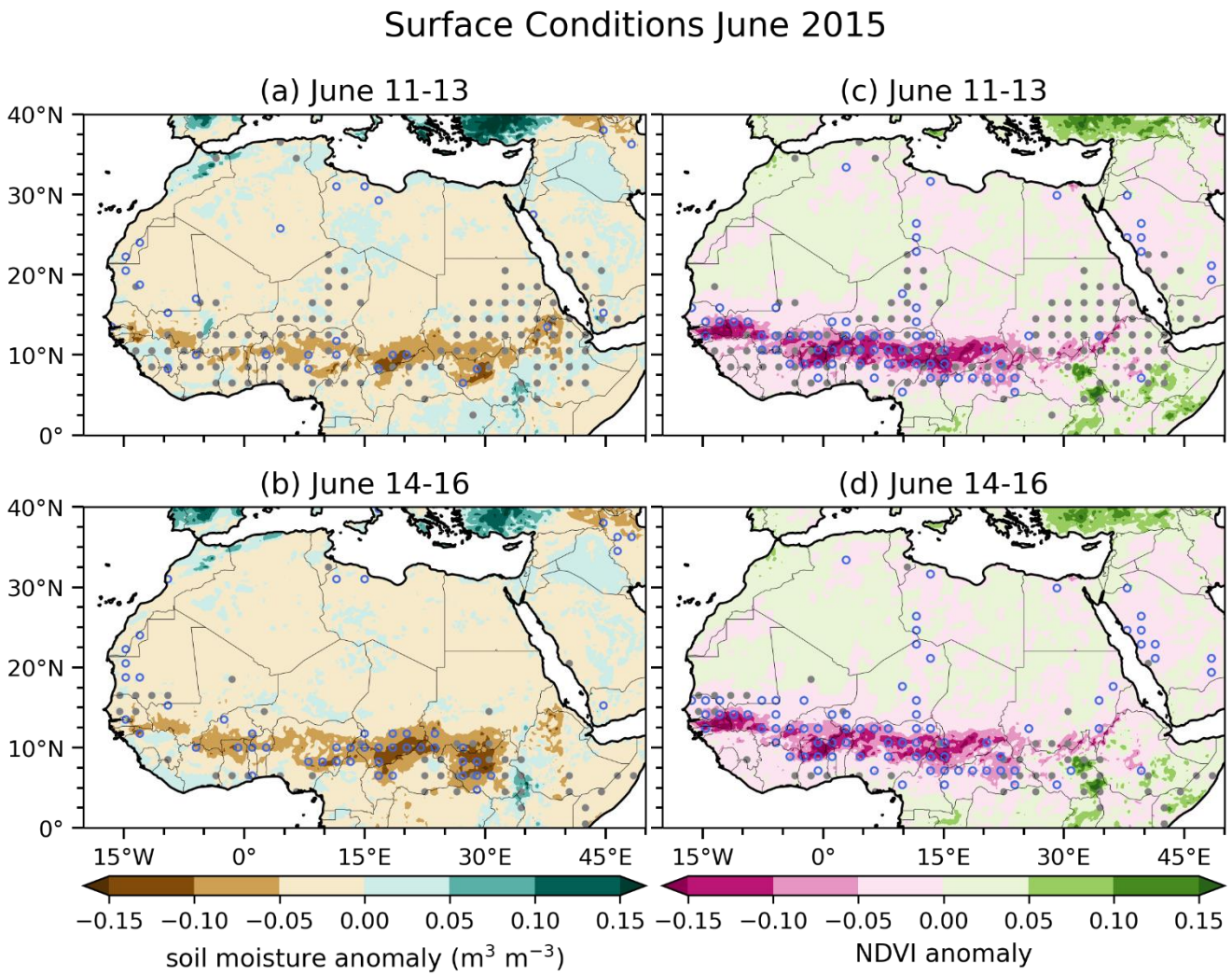

Figure 10. (a)-(b) Anomalies of ERA5 first-layer (top 7 cm) volumetric soil water ($m^3\ m^{-3}$; with reference to the 1979-2022 climatology in June) averaged over 11–13 June and 14–16 June 2015. Blue circles represent soil water ≤ 5th percentile (with respect to June three-day means from 2003-2022 at each grid point). (c)-(d) Anomalies of MODIS NDVI (with reference to the 2003-2022 climatology in June) averaged over 11–13 June and 14–16 June 14–16 2015. Blue circles represent NDVI ≤ 5th percentile (with respect to JJA three-day means from 2003-2022 at each grid point). Grey dots represent regions where MODIS AOD is ≥ 95th percentile (with reference to three-day mean MODIS AOD in JJA from 2003 to 2022 at each grid point) and ≥ 0.6.

4.4 Impacts of the 2015 trans-Atlantic extreme dust event

4.4.1 Radiation Impacts

The perturbation of the June 2015 extreme African dust plume on radiative fluxes at the TOA and surface is examined using CERES clear-sky daily data. Figure 11a shows anomalies of regional mean shortwave (SW) and longwave (LW) fluxes over the eastern tropical North Atlantic (8°N–25°N, 18°W–42°W), along with MODIS AOD in June 2015. At the surface, when

regional mean AOD reached the maximum of 1.1 on 16 June, the reduction of SW flux also reached a peak, at about –25.5 W m^{-2}, while LW flux had a weak warming anomaly of about 3.5 W m^{-2} associated with scattered and emitted LW radiation by the warm SAL. Consistent with previous studies (e.g., Tegen et al. 1996), changes in radiative fluxes at the TOA were much smaller than that at the surface, with about 1.0 W m^{-2} LW warming and –3.1 W m^{-2} SW cooling, although no clear maxima were found when AOD peaked. Both the sign and magnitude are consistent with previous studies of the TOA radiative effects of African dust over the Atlantic (e.g., Yu et al. 2006; Yorks et al. 2009). The SW cooling at the TOA is associated with the increased reflected solar flux due to the bright dust layer above the dark ocean surface, while the LW warming is often related to the absorption of outgoing LW by the dust layer but may be also affected by the moisture content in the atmosphere.

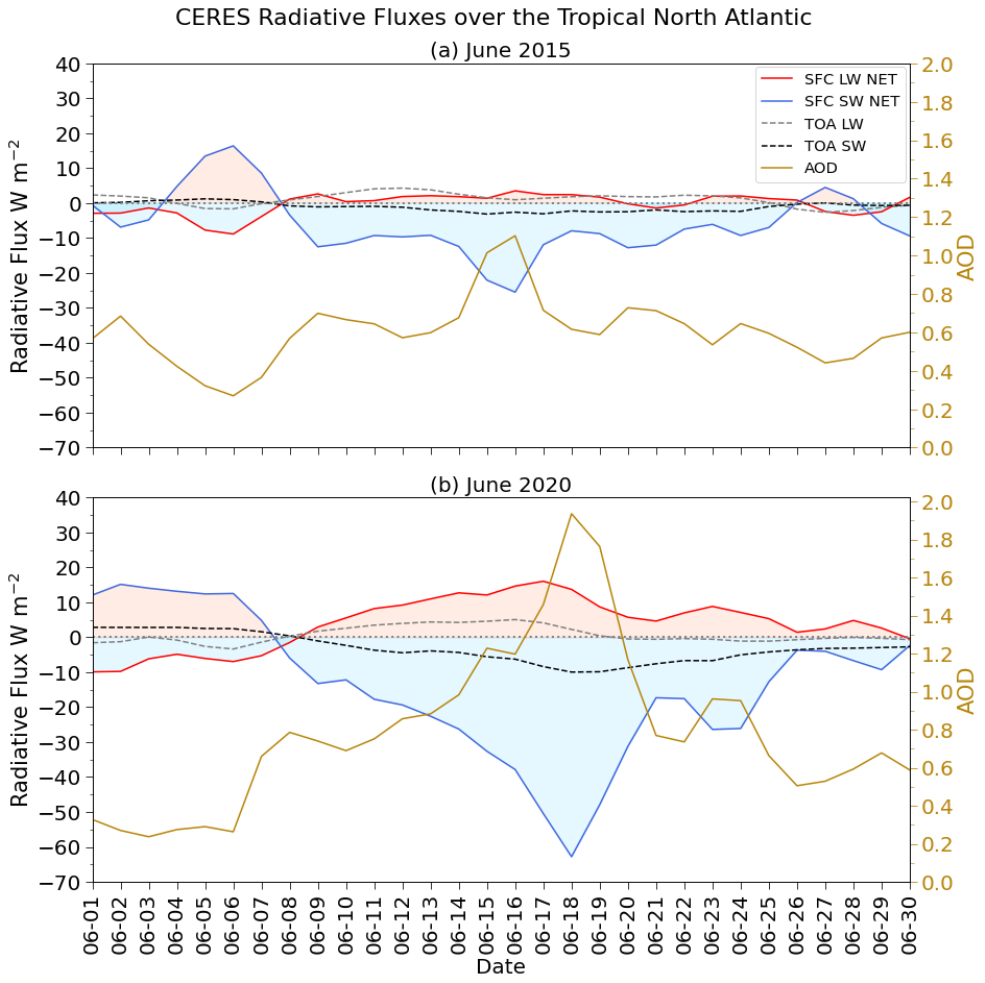

Figure 11. Time series of CERES clear-sky radiative fluxes (W m^{-2}) and MODIS AOD in (a) June 2015 and (b) June 2020 averaged over the eastern tropical North Atlantic between 8°N – 25°N and 18°W – 42°W. Anomalies (with reference to the 2003-2022 climatology in June) of net shortwave (SW) and longwave (LW) fluxes at the surface are shown in solid blue and red lines, respectively. Reflected SW and outgoing LW fluxes at the top of the atmosphere (TOA) are shown in dashed black and grey, respectively. Positive (negative) values indicate downward (upward) fluxes. Red (blue) shading denotes the warming (cooling) effect at the surface. AOD is shown in gold on the right y-axis.

Fig. 11b shows the radiative fluxes of the June 2020 event for comparison. With a more intense dust plume and a higher AOD of up to 1.9 on 18 June 2020, surface SW flux reached – 62.8 W m^{-2}, more than two times the perturbation in the June 2015 event. The corresponding surface LW flux perturbation is also about two times stronger. Also different from the June 2015 event is that the TOA SW flux showed a minimum (–9.9 W m^{-2}) when AOD reached a maximum, while the TOA LW warming effect peaked a bit early before the maximum of AOD. The net surface LW and SW flux values shown here are comparable to the changes in surface radiative fluxes over the eastern Atlantic found by Francis et al. (2022; their Fig. 4).

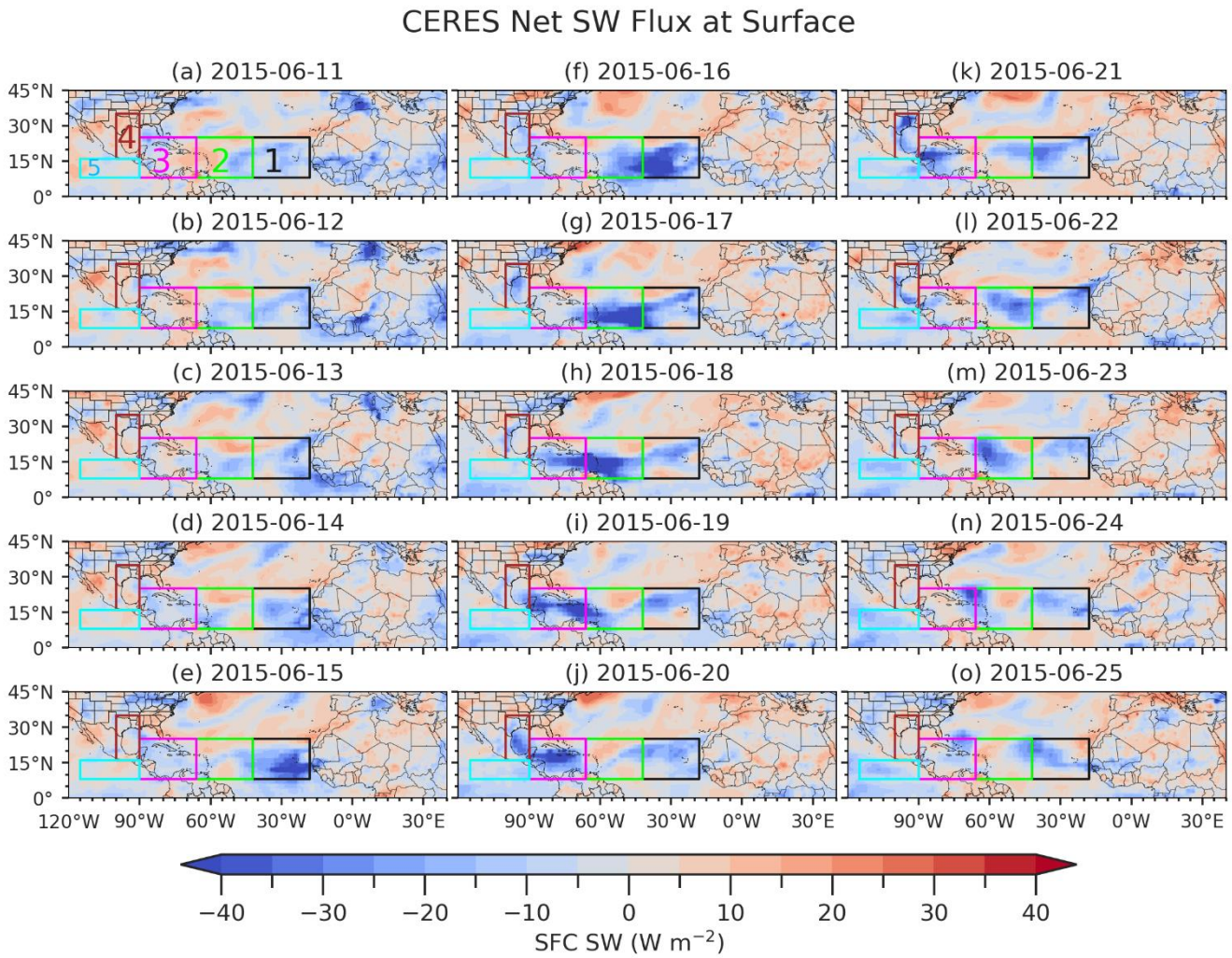

Figure 12. Anomalies (with reference to the June climatology over 2003-2022) of CERES clear-sky net shortwave fluxes at the surface (W m^{-2}). Boxes represent averaging regions to track the changes in radiative flux due to the propagation of the African dust plume. Region 1 (black) is between 8°N – 25°N and 18°W –42°W, Region 2 (green) is between 8°N – 25°N and 42°W – 66°W, Region 3 (magenta) is between 8°N –25°N and 66°W – 90°W, Region 4 (brown) is between 16°N – 35°N and 90°W – 100°W, and Region 5 (cyan) is between 8°N – 16°N and 90°W – 115°W.

The spatial pattern of anomalous net surface SW flux during the June 2015 event is shown in Figure 12. The propagation of the negative anomalies of surface SW fluxes is quite consistent with the westward movement of the dust plume (Fig. 3), as expected; and the large reductions are over the regions where AOD reached the 95th percentile (dotted areas in Fig. 3), with a magnitude of up to –73.6 W m^{-2} in the eastern tropical Atlantic on 16 June and reached -56.6 W m^{-2} over the Caribbean Basin on 21 June. Note that during 21–25 June, the reduction of surface net SW extended to the eastern tropical Pacific as the dust plume was advected to the region by the extremely strong CLLJ, with a magnitude of up to –28.4 W m^{-2}.

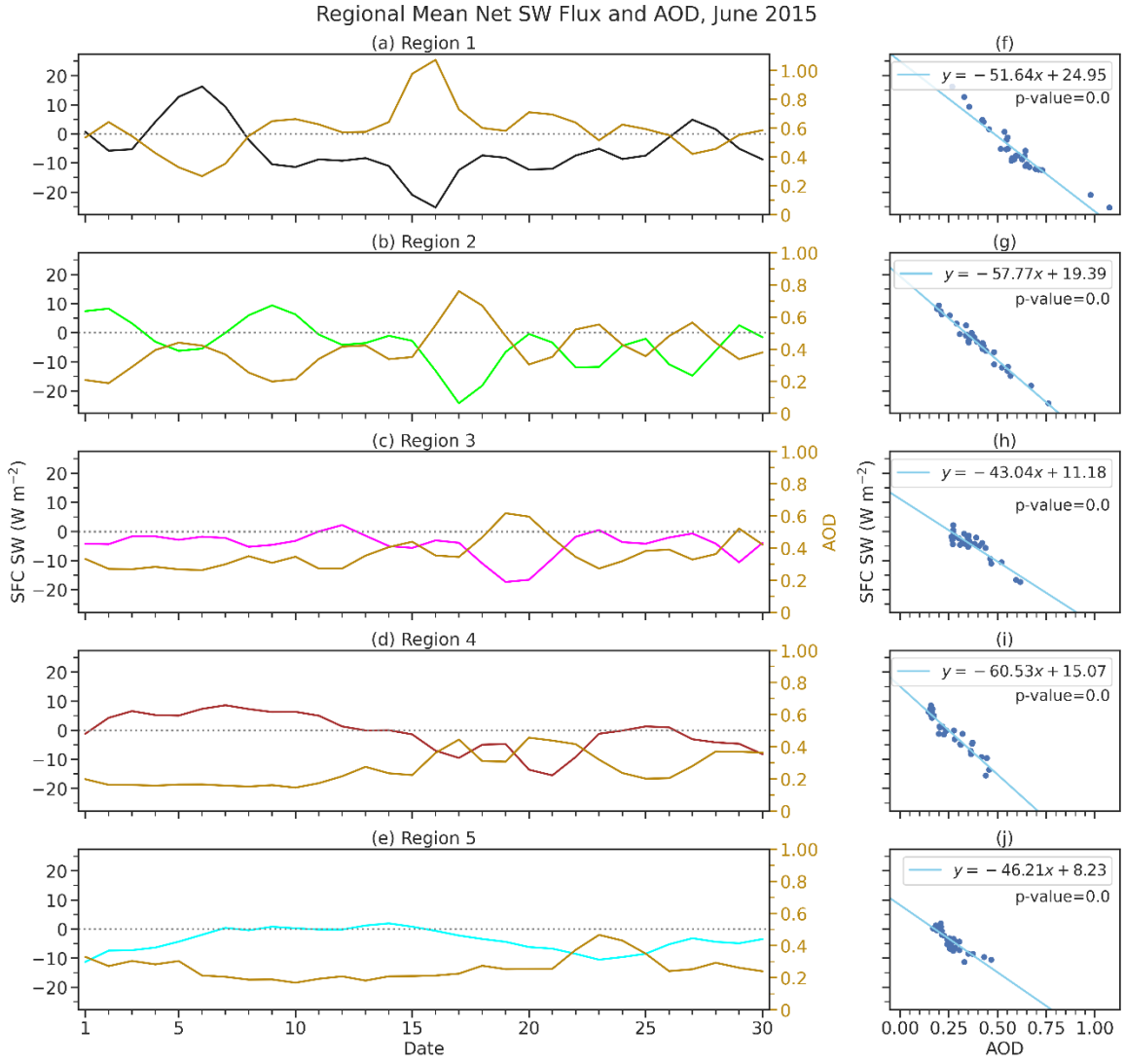

Figure 13. (a)-(e) Anomalies of CERES clear-sky net shortwave flux at the surface (with reference to the 2003-2022 climatology in June; W m^{-2}) over the tropical North Atlantic in Regions 1-5 (see locations in Fig. 12) in June 2015. Black, green, magenta, brown, and cyan lines are regional mean surface net shortwave flux from Regions 1–5. Golden lines show regional mean AOD in Regions 1–5. (f)-(j) Scatterplots of regional mean MODIS AOD versus anomalies of CERES clear-sky surface net shortwave fluxes (W m^{-2}) in Regions 1-5.

Figure 13 tracks the magnitude of surface net SW flux perturbation and its relationship to AOD by calculating regional averages of both variables within three subregions over the tropical North Atlantic (Regions 1–3; Fig. 12a), over the southeastern U.S. (Region 4) and over the tropical eastern Pacific (Region 5). Regions 1– 3 show a steady increase in AOD and a decline in anomalies of surface SW flux as the dust plume propagated westward (Fig. 13a-c). The previously described division of the dust plume resulted in higher regional AOD and lower SW flux in the Pacific (Region 5), while signals are much weaker in the southeastern U.S. due to a higher surface albedo over land (Region 4; Fig. 13d-e). The magnitude of surface SW perturbation is nearly linear with the magnitude of AOD in Regions 1-5 (Fig. 13f-j), about – 43.0 ± 7.9 (95% confidence intervals) to – 60.5 ± 7.6 W m^{-2} AOD^{-1}, similar to the nearly linear the relationship between increased AOD due to dust and perturbed TOA SW fluxes over the tropical North Atlantic found by previous studies, e.g., –36.5 ± 4.8 to –49.7 ± 7.1 W m^{-2} AOD^{-1} (Song et al., 2018). A similar linear relationship between AOD magnitude and surface net SW flux was found for the 2020 case (Figure S5), with 2020 showing slightly less negative coefficients in Regions 1 and 2, but slightly more negative in Region 3 in comparison with the 2015 event.

The anomalies of surface net LW fluxes versus AOD in the June 2015 event are shown in Figure S6. A nearly linear relationship between AOD and net LW fluxes was also found over the tropical North Atlantic (Regions 1-2), but not over the Caribbean Basin (Region 3), likely being interfered with by other factors modifying surface longwave flux, such as low-level moisture content and SST.

4.4.2 Air Quality Impacts

The air quality impacts of the 2015 trans-Atlantic dust plume seem to be minor in the United States. Figure 14 shows the daily $PM_{2.5}$ concentration and Air Quality Index (AQI) from 20 to 25 June 2015. $PM_{2.5}$ concentrations increased as the dust plume arrived in the Gulf states around 21 June, propagated northward to the central U.S. and southern Midwest states on 23 June, and eventually decayed around 25 June (Figs. 14 b-f). While $PM_{2.5}$ measurements are well within the U.S. Environmental Protection Agency (EPA) standard of 35 μg m^{-3}, some sites over Texas, Oklahoma, Kansas, Louisiana, Mississippi, Alabama, Georgia, Tennessee, and West Virginia show $PM_{2.5}$ concentration exceeded the World Health Organization (WHO) air quality guidelines of 25 μg m^{-3} (2005 standard) during the event, with the strongest impacts on 23 June (Fig. 14d). Even more states reached the latest WHO guideline of 15 μg m^{-3} (2021 standard), but likely also revealing the impacts of other aerosols (e.g., local anthropogenic emissions). Chen et al. (2018) also found four sites in Texas reported daily maximum $PM_{2.5}$ concentrations above 36.3 μg m^{-3} due to the long-range transported African dust from 21-23 June 2015.

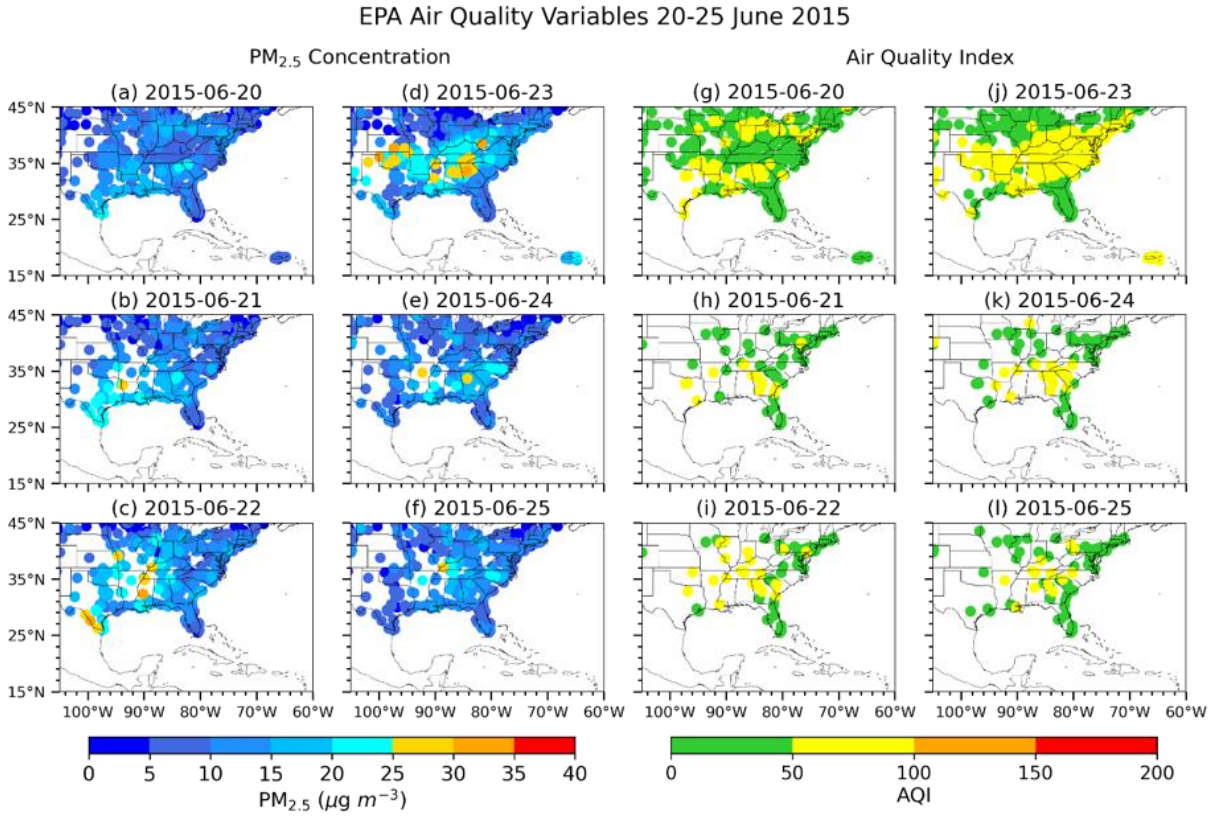

Figure 14. (a)-(f) Daily $PM_{2.5}$ concentrations (μg m^{-3}) and (g)-(l) Air Quality Index (AQI) from EPA Air Quality System (AQS) stations from 20 to 25 June 2015. AQI values of 0–50 indicate good air quality (green), 51–100 for moderate condition (yellow), 101–150 for unhealthy for sensitive groups (orange), and 151–200 for unhealthy condition (red).

AQI gives a similar story with all daily ratings being in the "Good" (green) to "Moderate" (yellow) range (Figs. 14g-l). The relatively weak perturbation of the African dust plume on AQI and $PM_{2.5}$ records in the June 2015 event is associated with the extremely strong CLLJ during 17–25 June that dispersed the part of the plume to the eastern Pacific, which greatly reduced the amount of dust to the continental U.S. This suggests that air quality impacts of African dust in the U.S. are sensitive to local circulations such as the CLLJ, in addition to the amount of transported dust over the tropical North Atlantic.

4.5 Comparison to the 2020 extreme trans-Atlantic dust event

In this section, we further compare the June 2015 event with the extreme "Godzilla" dust event in June 2020. The evolution of both events was quite similar. The extremely high AOD over the tropical North Atlantic was led by a great intensification of the AEJ two to four days ahead of time, while the enhancement of the CLLJ and AOD over the Caribbean Basin was almost concurrent (Fig. S7). Note that in both cases the AEJ increased again after the extreme trans-Atlantic dust events we focused on, e.g., around 21–23 June 2015 and 24–28 June 2020, consistent with the formation of another trans-Atlantic African dust plume (Fig. 3 here and Fig. 1 of Pu and Jin 2021).

The peak magnitude of regional mean MODIS AOD in the tropical North Atlantic was lower in 2015 (0.71) than they were in 2020 (1.01; Fig. S7a), consistent with the lower peak value of AOD over western North Africa (0.74 vs. 1.02). The peak magnitude of AOD over the Caribbean Basin in the 2015 case is also lower than that of 2020 (0.66 vs. 0.96), along with a stronger CLLJ in the 2015 event (Fig. S7b) that advected a portion of the dust plume away to the eastern Pacific, resulting in much weaker air quality impacts in the 2015 event than that of the 2020 event. Table 1 summarizes the magnitude and duration of the AEEs of the two events along with the radiative and air quality impacts. Consistent with the weaker magnitude and shorter duration of the AEEs in the June 2015 event, the resultant perturbations of radiative fluxes over the eastern tropical Atlantic and air quality over the southeastern U.S. are weaker in the 2015 event.

In terms of dust emissions, increased surface wind speeds in dust source regions over western North Africa and favorable land surface conditions, such as soil moisture deficit and vegetation decay in the Sahel, are found in both events (Table 2). However, the magnitude and duration of AEE over western North Africa in the 2015 event (0.74, one day) is much weaker than that of the 2020 event (0.90, six days). In fact, the magnitude of African AEE in the 2015 event is very close to the mean of all the summertime AEEs during 2003–2022 (0.73; Fig. 1d). The quite moderate AEE in the dust source regions and the disproportionally high dust loading over the tropical North Atlantic (i.e., the second strongest AEE following the 2020 event) suggests the importance of atmospheric circulation conditions that facilitate the westward transport of African dust to the ocean, i.e., the extremely intensified AEJ (with a magnitude comparable to that during the 2020 event; Table 2) and CLLJ (greater than that of the 2020 event; Table 2), along with the intensified and westward extended NASH.

Table 1. The features and impacts of the extreme trans-Atlantic dust events in June 2015 and June 2020. The magnitude and duration (in brackets) of the AEEs over both the tropical North Atlantic (TNA; green box in Fig. 1a) and western North Africa (WNA; blue box in Fig. 1a) are listed. The corresponding regional mean DOD from the MERRA-2 during the same periods is shown in square brackets. The peak perturbation of the shortwave (SW) and long wave (LW) radiative fluxes at the surface (sfc) and top of the atmosphere (TOA) averaged over the eastern tropical North Atlantic (box 1 in Fig. 12) during the corresponding AEE_{TNA} events are shown. Values are shown in anomalies with reference to the June climatology during 2003–2022. The last two columns show the numbers of states over the southeastern U.S. (24–40°N; 74–105°W) with $PM_{2.5}$ concentrations exceeding the EPA guideline of 35 μg m^{-3} and with AQI > 100 during the peak pollutant days of the two events (i.e., 23 June 2015 and 27 June 2020), respectively.

Events	Magnitude and Duration (days)		Radiative fluxes (W m^{-2})				Air Quality (states)	
	AEE_{TNA}	AEE_{WNA}	SW_{sfc}	LW_{sfc}	SW_{TOA}	LW_{TOA}	$PM_{2.5}$ > 35 μg m^{-3}	AQI>100
2015	0.61 [0.28] (6)	0.74 [0.52] (1)	-25.5	3.5	-3.2	1.0	0	0
2020	0.77 [0.43] (12)	0.90 [0.88] (6)	-62.8	16.1	-9.9	5.1	12	12

Table 2. A comparison of the land surface and circulation conditions between the June 2015 and June 2020 extreme trans-Atlantic dust events. Surface wind speed (V_{10m}), NDVI, and soil moisture over the dust source region in western North Africa (blue box in Fig. 1a) are calculated in a two-week period for each event, i.e., before the onset of the event to the early stage of the event (3–16 June 2015 and 7–20 June 2020). Values are shown in anomalies with reference to the June climatology during 2003–2022. The magnitude of the AEJ index in both events is calculated during the whole event (i.e., 12–23 June 2015 and 14–27 June 2020). The magnitude of the CLLJ index and regional mean 850 hPa geopotential height (Z_{850}) over the western NASH (17°–35°N, 70°–95°W) are calculated over the late stages of each event (17–23 June 2015 and 21–27 June 2020), i.e., when the plume arrived at the western tropical North Atlantic. All the circulation variables are shown in anomalies with reference to the June climatology over 1979–2022 in the ERA5. The percentages of the anomalies with reference to the climatological means are shown in brackets.

Events	V_{10m} (m s^{-1})	NDVI	Soil moisture (m^3 m^{-3})	AEJ (m s^{-1})	Z_{850} (gpm)	CLLJ (m s^{-1})
2015	0.74 (24.2%)	-0.03 (-10.0%)	-0.016 (-15.9%)	16.35 (27.4%)	26.7 (1.7%)	18.2 (47.1%)
2020	1.1 (35.7%)	-0.02 (-7.4%)	-0.005 (-4.5%)	16.32 (27.2%)	20.6 (1.3%)	16.8 (35.8%)

5 Discussion

Several uncertainties are associated with the analysis of the June 2015 extreme African dust event. We mainly use satellite retrievals, i.e., MODIS and VIIRS, to examine the magnitude of the event. Since AOD at 550 nm from the polar-orbiting satellites is only available one time daily, with areas of missing values due to clouds or retrieval uncertainties, the magnitude of the dust plume may be underestimated as sub-daily variations are not able to be captured. This is also revealed by the comparison between satellite AOD with AERONET sub-daily AOD during the event (Fig. 4). The daytime maxima recorded by ground observations were largely missed by MODIS and VIIRS AOD. On the other hand, AERONET records also have drawbacks such as limited spatial coverage, e.g., very few sites over the central to eastern tropical North Atlantic, thus combining both datasets provides a better characterization of the event.

We found that the extremely high loading of dust over the tropical North Atlantic is due to a moderate increase of African dust emissions and strongly enhanced AEJ, NASH, and CLLJ over the tropical North Atlantic and Caribbean Basin that advected African dust westward. While previous modelling studies show that African dust aerosols can lead to a higher, northward displaced, and intensified AEJ via their radiative effects (e.g., Wilcox et al. 2010; Reale et al. 2011; Grogan et al. 2017; Bercos-Hickey et al. 2017, 2020), to what extent the extreme dust plume may affect the circulation patterns and consequently feedback to its westward propagation is not fully clear in our observational study and warrants further examination in the future.

While CERES TOA radiative fluxes are from satellite retrievals, it should be noted that the surface radiative fluxes are from the radiative transfer model and the results of which are sensitive to prescribed aerosol optical properties, assimilated satellite cloud properties and MODIS AOD. Improved understanding of dust optical properties, such as dust mineralogy from global dust source regions made available by the Earth Surface Mineral Dust Source Investigation (EMIT) mission (Green et al., 2020), will greatly reduce uncertainties related to the radiative effects of extreme trans-Atlantic African dust events and will be explored in future studies.

6 Conclusion

This research seeks to improve the current understanding of extreme trans-Atlantic dust storms by examining the causes and impacts of the second strongest summertime trans-Atlantic African dust event from 2003 to 2022. The June 2015 event was characterized by a one-day aerosol extreme event (AEE) over the dust source regions in western North Africa on 13 June and a six-day AEE over the tropical North Atlantic from 15 to 20 June. The enhanced dust emissions over land are associated with the extremely strong surface wind speeds over western North Africa in Mauritania and Mali and soil moisture deficit and vegetation decay in the southern Sahel. The greatly intensified African easterly jet (AEJ) over West Africa and the eastern tropical North Atlantic from 11–16 June transported a large amount of African dust toward the ocean. From the western tropical North Atlantic to the Gulf of Mexico, the westward extension of the North Atlantic subtropical high (NASH) further advected the dust plume westward. The increased meridional height gradient over the Caribbean Basin resulted in an extremely enhanced Caribbean low-level jet (CLLJ) that further transported the dust plume westward. The anomalously strong easterly jet diverted a portion of the dust plume westward to the eastern tropical Pacific, while the anticyclonic flow of the NASH steered the rest of the plume to the southern U.S.

The dense dust plume reduced the regional mean surface net shortwave flux by about 25.3 W m^{-2} (17.3 W m^{-2}) and increased the net surface longwave by about 3.5 W m^{-2} (3.1 W m^{-2}) over the tropical eastern Atlantic (the Caribbean Basin). Over the tropical eastern Pacific (8°N – 16°N, 90°W – 115°W), a reduction of regional mean net surface shortwave flux by 10.5 W m^{-2} and an increase in longwave of 5.6 W m^{-2} are also found as the dust plume was transported to the region by the extremely strong CLLJ. The arrival of the African dust plume increased $PM_{2.5}$ concentrations over the southern U.S. during 21–25 June. The pollution was the strongest on 23 June, when daily $PM_{2.5}$ concentrations at some sites over Texas, Oklahoma, Kansas, Mississippi, Alabama, Georgia, Tennessee, and West Virginia exceeded 25 μg m^{-3}. However, none of the sites show a daily mean above the EPA guideline of 35 μg m^{-3}. The air quality index (AQI) never exceeded 100 but was elevated to 51-100 or a "moderate" level for many states. The overall air quality impacts are not particularly dangerous, likely due to the strengthened CLLJ that deflected part of the African dust plume into the Pacific, resulting in a lower dust loading in the southern U.S.

Similar to the "Godzilla" dust event in June 2020, i.e., the strongest trans-Atlantic African dust event in JJA since 2003, circulation extremes also played important roles in the formation of the 2015 extreme trans-Atlantic dust event. Although the magnitude and duration of the dust emissions in the 2015 event are much weaker than the 2020 event, i.e., a one-day AEE with a magnitude close to the long-term mean of summertime AEEs, the extremely intensified AEJ (the fourth strongest for 11–16 June over 1979–2022) and CLLJ (the strongest for 17–22 June over 1979–2022) and the enhanced (geopotential height reached 95th percentile in June over 1979–2022) and westward extended NASH, all facilitate the westward transport of African dust to the ocean, resulting in a disproportionally high (the second strongest in summer since 2003) dust loading over the tropical North Atlantic. Understanding the mechanisms and impacts of extreme trans-Atlantic African dust events like those in 2015 and 2020 is crucial for predicting slimier extreme dust events and mitigating their negative effects on weather, climate,

air quality, and human health. This analysis reveals the importance of atmospheric circulation features over the tropical North Atlantic and the Caribbean Basin, like the NASH, AEJ, and CLLJ, in influencing the westward transportation and dispersion of African dust plumes and how that changes the impacts of extreme dust events.

Code availability

Analysis codes can be provided upon request from the corresponding authors.

Data availability

ERA5 hourly and monthly data at single and pressure levels can be downloaded at https://cds.climate.copernicus.eu/#!/home. MERRA-2 DOD can be downloaded from https://disc.gsfc.nasa.gov/datasets?keywords=MERRA-2&page=1. MODIS AOD can be obtained from https://ladsweb.modaps.eosdis.nasa.gov/search/. IMERG sub-hourly precipitation can be downloaded at https://disc.gsfc.nasa.gov/datasets/GPM_3IMERGHH_06/summary. CALIOP lidar can be downloaded from https://asdc.larc.nasa.gov/project/CALIPSO/CAL_LID_L3_Tropospheric_APro_CloudFree-Standard-V4-20_V4-20. CERES radiation fluxes were obtained from the NASA Langley Research Center CERES ordering tool at https://asdc.larc.nasa.gov/project/CERES/CERES_EBAF_Edition4.2. AERONET station data can be acquired at https://aeronet.gsfc.nasa.gov/. EPA air quality data can be found at https://www.epa.gov/outdoor-air-quality-data/download-daily-data, and SEVIRI dust RGB data are available at https://eumetsatspace.atlassian.net/wiki/spaces/EUM/overview.

Author contributions

The study was conceived by BP. BH performed the analysis with guidance and assistance from BP and QJ. BH wrote the paper with input and edits from BP and QJ.

Competing interests

The authors declare no competing interests.

Acknowledgements

We thank David Mechem and Nathaniel Brunsell for their helpful suggestions for this paper. We also thank Jacob Tindan for his assistance with coding in the early stages of the study. The helpful comments from four anonymous reviewers greatly improved the paper and are sincerely appreciated.

Financial support

This research has been supported by the National Science Foundation (grant no. AGS-2227707).

690

695

700

References

Ackerman, S. A.: Remote sensing aerosols using satellite infrared observations, J. Geophys. Res. Atmospheres, 102, 17069–17079, https://doi.org/10.1029/96JD03066, 1997.

705 Adams, A. M., Prospero, J. M., and Zhang, C.: CALIPSO-Derived Three-Dimensional Structure of Aerosol over the Atlantic Basin and Adjacent Continents, J. Clim., 25, 6862–6879, https://doi.org/10.1175/JCLI-D-11-00672.1, 2012.

Agutu, N. O., Ndehedehe, C. E., Awange, J. L., Kirimi, F., and Mwaniki, M.: Understanding uncertainty of model-reanalysis soil moisture within Greater Horn of Africa (1982–2014), J. Hydrol., 603, 127169, https://doi.org/10.1016/j.jhydrol.2021.127169, 2021.

710 Akpinar-Elci, M., Martin, F. E., Behr, J. G., and Diaz, R.: Saharan dust, climate variability, and asthma in Grenada, the Caribbean, Int. J. Biometeorol., 59, 1667–1671, https://doi.org/10.1007/s00484-015-0973-2, 2015.

Ashpole, I. and Washington, R.: An automated dust detection using SEVIRI: A multiyear climatology of summertime dustiness in the central and western Sahara, J. Geophys. Res. Atmospheres, 117, https://doi.org/10.1029/2011JD016845, 2012.

Asutosh, A., Vinoj, V., Murukesh, N., Ramisetty, R., and Mittal, N.: Investigation of June 2020 giant Saharan dust storm using
715 remote sensing observations and model reanalysis, Sci. Rep., 12, 6114, https://doi.org/10.1038/s41598-022-10017-1, 2022.

Banks, J. R., Schepanski, K., Heinold, B., Hünerbein, A., and Brindley, H. E.: The influence of dust optical properties on the colour of simulated MSG-SEVIRI Desert Dust infrared imagery, Atmospheric Chem. Phys., 18, 9681–9703, https://doi.org/10.5194/acp-18-9681-2018, 2018.

Banks, J. R., Hünerbein, A., Heinold, B., Brindley, H. E., Deneke, H., and Schepanski, K.: The sensitivity of the colour of dust in MSG-SEVIRI Desert Dust infrared composite imagery to surface and atmospheric conditions, Atmospheric Chem. Phys., 19, 6893–6911, https://doi.org/10.5194/acp-19-6893-2019, 2019.

Barkan, J., Kutiel, H., Alpert, P., and Kishcha, P.: Synoptics of dust intrusion days from the African continent into the Atlantic Ocean, J. Geophys. Res. Atmospheres, 109, https://doi.org/10.1029/2003JD004416, 2004.

Beck, H. E., Pan, M., Miralles, D. G., Reichle, R. H., Dorigo, W. A., Hahn, S., Sheffield, J., Karthikeyan, L., Balsamo, G., Parinussa, R. M., van Dijk, A. I. J. M., Du, J., Kimball, J. S., Vergopolan, N., and Wood, E. F.: Evaluation of 18 satellite- and model-based soil moisture products using in situ measurements from 826 sensors, Hydrol. Earth Syst. Sci., 25, 17–40, https://doi.org/10.5194/hess-25-17-2021, 2021.

Bercos-Hickey, E., Nathan, T. R., and Chen, S.-H.: Saharan dust and the African easterly jet–African easterly wave system: Structure, location and energetics, Q. J. R. Meteorol. Soc., 143, 2797–2808, https://doi.org/10.1002/qj.3128, 2017.

Bercos-Hickey, E., Nathan, T. R., and Chen, S.-H.: On the Relationship between the African Easterly Jet, Saharan Mineral Dust Aerosols, and West African Precipitation, J. Clim., 33, 3533–3546, https://doi.org/10.1175/JCLI-D-18-0661.1, 2020.

Bozlaker, A., Prospero, J. M., Price, J., and Chellam, S.: Identifying and Quantifying the Impacts of Advected North African Dust on the Concentration and Composition of Airborne Fine Particulate Matter in Houston and Galveston, Texas, J. Geophys. Res. Atmospheres, 124, 12282–12300, https://doi.org/10.1029/2019JD030792, 2019.

Braun, S. A.: Reevaluating the Role of the Saharan Air Layer in Atlantic Tropical Cyclogenesis and Evolution, Mon. Weather Rev., 138, 2007–2037, https://doi.org/10.1175/2009MWR3135.1, 2010.

Brindley, H., Knippertz, P., Ryder, C., and Ashpole, I.: A critical evaluation of the ability of the Spinning Enhanced Visible and Infrared Imager (SEVIRI) thermal infrared red-green-blue rendering to identify dust events: Theoretical analysis, J. Geophys. Res. Atmospheres, 117, https://doi.org/10.1029/2011JD017326, 2012.

Brindley, H. E. and Russell, J. E.: An assessment of Saharan dust loading and the corresponding cloud-free longwave direct radiative effect from geostationary satellite observations, J. Geophys. Res. Atmospheres, 114, https://doi.org/10.1029/2008JD011635, 2009.

Bristow, C. S., Hudson-Edwards, K. A., and Chappell, A.: Fertilizing the Amazon and equatorial Atlantic with West African dust, Geophys. Res. Lett., 37, https://doi.org/10.1029/2010GL043486, 2010.

Brocca, L., Massari, C., Pellarin, T., Filippucci, P., Ciabatta, L., Camici, S., Kerr, Y. H., and Fernández-Prieto, D.: River flow prediction in data scarce regions: soil moisture integrated satellite rainfall products outperform rain gauge observations in West Africa, Sci. Rep., 10, 12517, https://doi.org/10.1038/s41598-020-69343-x, 2020.

Buchard, V., Randles, C. A., Silva, A. M. da, Darmenov, A., Colarco, P. R., Govindaraju, R., Ferrare, R., Hair, J., Beyersdorf, A. J., Ziemba, L. D., and Yu, H.: The MERRA-2 Aerosol Reanalysis, 1980 Onward. Part II: Evaluation and Case Studies, J. Clim., 30, 6851–6872, https://doi.org/10.1175/JCLI-D-16-0613.1, 2017.

Burpee, R. W.: The Origin and Structure of Easterly Waves in the Lower Troposphere of North Africa, J. Atmospheric Sci., 29, 77–90, https://doi.org/10.1175/1520-0469(1972)029<0077:TOASOE>2.0.CO;2, 1972.

CALIPSO User Guide: https://www-calipso.larc.nasa.gov/resources/calipso_users_guide/data_summaries/profile_data_v420.php#heading09, last access: 30 March, 2024, last update: 2018.

Carlson, T. N. and Caverly, R. S.: Radiative characteristics of Saharan dust at solar wavelengths, J. Geophys. Res. 1896-1977, 82, 3141–3152, https://doi.org/10.1029/JC082i021p03141, 1977.

Carlson, T. N. and Prospero, J. M.: The Large-Scale Movement of Saharan Air Outbreaks over the Northern Equatorial Atlantic, J. Appl. Meteorol. Climatol., 11, 283–297, https://doi.org/10.1175/1520-0450(1972)011<0283:TLSMOS>2.0.CO;2, 1972.

Caton Harrison, T., Washington, R., and Engelstaedter, S.: Satellite-Derived Characteristics of Saharan Cold Pool Outflows During Boreal Summer, J. Geophys. Res. Atmospheres, 126, e2020JD033387, https://doi.org/10.1029/2020JD033387, 2021.

Chen, S.-P., Lu, C.-H., McQueen, J., and Lee, P.: Application of satellite observations in conjunction with aerosol reanalysis to characterize long-range transport of African and Asian dust on air quality in the contiguous U.S., Atmos. Environ., 187, 174–195, https://doi.org/10.1016/j.atmosenv.2018.05.038, 2018.

Claquin, T., Roelandt, C., Kohfeld, K., Harrison, S., Tegen, I., Prentice, I., Balkanski, Y., Bergametti, G., Hansson, M., Mahowald, N., Rodhe, H., and Schulz, M.: Radiative forcing of climate by ice-age atmospheric dust, Clim. Dyn., 20, 193–202, https://doi.org/10.1007/s00382-002-0269-1, 2003.

Cook, K. H.: Generation of the African Easterly Jet and Its Role in Determining West African Precipitation, J. Clim., 12, 1165–1184, https://doi.org/10.1175/1520-0442(1999)012<1165:GOTAEJ>2.0.CO;2, 1999.

Cowie, S. M., Knippertz, P., and Marsham, J. H.: A climatology of dust emission events from northern Africa using long-term surface observations, Atmospheric Chem. Phys., 14, 8579–8597, https://doi.org/10.5194/acp-14-8579-2014, 2014.

Cowie, S. M., Marsham, J. H., and Knippertz, P.: The importance of rare, high-wind events for dust uplift in northern Africa, Geophys. Res. Lett., 42, 8208–8215, https://doi.org/10.1002/2015GL065819, 2015.

DeMott, P. J., Sassen, K., Poellot, M. R., Baumgardner, D., Rogers, D. C., Brooks, S. D., Prenni, A. J., and Kreidenweis, S. M.: African dust aerosols as atmospheric ice nuclei, Geophys. Res. Lett., 30, https://doi.org/10.1029/2003GL017410, 2003.

Didan, K., Munoz, A. B., and Huete, A.: MODIS Vegetation Index User's Guide (MOD13 Series), n.d.

Doelling, D. R., Sun, M., Nguyen, L. T., Nordeen, M. L., Haney, C. O., Keyes, D. F., and Mlynczak, P. E.: Advances in Geostationary-Derived Longwave Fluxes for the CERES Synoptic (SYN1deg) Product, J. Atmospheric Ocean. Technol., 33, 503–521, https://doi.org/10.1175/JTECH-D-15-0147.1, 2016.

Doherty, O. M., Riemer, N., and Hameed, S.: Saharan mineral dust transport into the Caribbean: Observed atmospheric controls and trends, J. Geophys. Res. Atmospheres, 113, https://doi.org/10.1029/2007JD009171, 2008.

Dunion, J. P.: Rewriting the Climatology of the Tropical North Atlantic and Caribbean Sea Atmosphere, J. Clim., 24, 893–908, https://doi.org/10.1175/2010JCLI3496.1, 2011.

Dunion, J. P. and Velden, C. S.: The Impact of the Saharan Air Layer on Atlantic Tropical Cyclone Activity, Bull. Am. Meteorol. Soc., 85, 353–366, https://doi.org/10.1175/BAMS-85-3-353, 2004.

Engelstaedter, S. and Washington, R.: Atmospheric controls on the annual cycle of North African dust, J. Geophys. Res. Atmospheres, 112, https://doi.org/10.1029/2006JD007195, 2007.

Engelstaedter, S., Tegen, I., and Washington, R.: North African dust emissions and transport, Earth-Sci. Rev., 79, 73–100, https://doi.org/10.1016/j.earscirev.2006.06.004, 2006.

Española, S., Urrutia-Pereira, M., Rizzo, L., Staffeld, P., Chong Neto, H., Viegi, G., and Solé, D.: P U B L I C A T I O N S CODON Allergologia et immunopathologia Dust from the Sahara to the American Continent: Health impacts, Allergol. Immunopathol. (Madr.), 49, 187–194, https://doi.org/10.15586/aei.v49i4.436, 2021.

Evan, A. T., Flamant, C., Gaetani, M., and Guichard, F.: The past, present and future of African dust, Nature, 531, 493–495, https://doi.org/10.1038/nature17149, 2016.

Fiedler, S., Kaplan, M. L., and Knippertz, P.: The importance of Harmattan surges for the emission of North African dust aerosol, Geophys. Res. Lett., 42, 9495–9504, https://doi.org/10.1002/2015GL065925, 2015.

Foltz, G. R., Evan, A. T., Freitag, H. P., Brown, S., and McPhaden, M. J.: Dust Accumulation Biases in PIRATA Shortwave Radiation Records, J. Atmospheric Ocean. Technol., 30, 1414–1432, https://doi.org/10.1175/JTECH-D-12-00169.1, 2013.

Fontaine, B., Philippon, N., Trzaska, S., and Roucou, P.: Spring to summer changes in the West African monsoon through NCEP/NCAR reanalyses (1968–1998), J. Geophys. Res. Atmospheres, 107, ACL 1-1-ACL 1-9, https://doi.org/10.1029/2001JD000834, 2002.

Francis, D., Fonseca, R., Nelli, N., Cuesta, J., Weston, M., Evan, A., and Temimi, M.: The Atmospheric Drivers of the Major Saharan Dust Storm in June 2020, Geophys. Res. Lett., 47, e2020GL090102, https://doi.org/10.1029/2020GL090102, 2020.

Francis, D., Nelli, N., Fonseca, R., Weston, M., Flamant, C., and Cherif, C.: The dust load and radiative impact associated with the June 2020 historical Saharan dust storm, Atmos. Environ., 268, 118808, https://doi.org/10.1016/j.atmosenv.2021.118808, 2022.

Freitas, E. da S., Coelho, V. H. R., Xuan, Y., Melo, D. de C. D., Gadelha, A. N., Santos, E. A., Galvão, C. de O., Ramos Filho, G. M., Barbosa, L. R., Huffman, G. J., Petersen, W. A., and Almeida, C. das N.: The performance of the IMERG satellite-based product in identifying sub-daily rainfall events and their properties, J. Hydrol., 589, 125128, https://doi.org/10.1016/j.jhydrol.2020.125128, 2020.

Gelaro, R., McCarty, W., Suárez, M. J., Todling, R., Molod, A., Takacs, L., Randles, C. A., Darmenov, A., Bosilovich, M. G., Reichle, R., Wargan, K., Coy, L., Cullather, R., Draper, C., Akella, S., Buchard, V., Conaty, A., Silva, A. M. da, Gu, W., Kim, G.-K., Koster, R., Lucchesi, R., Merkova, D., Nielsen, J. E., Partyka, G., Pawson, S., Putman, W., Rienecker, M., Schubert, S. D., Sienkiewicz, M., and Zhao, B.: The Modern-Era Retrospective Analysis for Research and Applications, Version 2 (MERRA-2), J. Clim., 30, 5419–5454, https://doi.org/10.1175/JCLI-D-16-0758.1, 2017.

Giles, D. M., Sinyuk, A., Sorokin, M. G., Schafer, J. S., Smirnov, A., Slutsker, I., Eck, T. F., Holben, B. N., Lewis, J. R., Campbell, J. R., Welton, E. J., Korkin, S. V., and Lyapustin, A. I.: Advancements in the Aerosol Robotic Network (AERONET) Version 3 database – automated near-real-time quality control algorithm with improved cloud screening for Sun photometer aerosol optical depth (AOD) measurements, Atmospheric Meas. Tech., 12, 169–209, https://doi.org/10.5194/amt-12-169-2019, 2019.

Gillette, D. A., Adams, J., Endo, A., Smith, D., and Kihl, R.: Threshold velocities for input of soil particles into the air by desert soils, J. Geophys. Res. Oceans, 85, 5621–5630, https://doi.org/10.1029/JC085iC10p05621, 1980.

Goudie, A. S.: Desert dust and human health disorders, Environ. Int., 63, 101–113, https://doi.org/10.1016/j.envint.2013.10.011, 2014.

Goudie, A. S. and Middleton, N. J.: Saharan dust storms: nature and consequences, Earth-Sci. Rev., 56, 179–204, https://doi.org/10.1016/S0012-8252(01)00067-8, 2001.

Green, R. O., Mahowald, N., Ung, C., Thompson, D. R., Bator, L., Bennet, M., Bernas, M., Blackway, N., Bradley, C., Cha, J., Clark, P., Clark, R., Cloud, D., Diaz, E., Ben Dor, E., Duren, R., Eastwood, M., Ehlmann, B. L., Fuentes, L., Ginoux, P., Gross, J., He, Y., Kalashnikova, O., Kert, W., Keymeulen, D., Klimesh, M., Ku, D., Kwong-Fu, H., Liggett, E., Li, L., Lundeen, S., Makowski, M. D., Mazer, A., Miller, R., Mouroulis, P., Oaida, B., Okin, G. S., Ortega, A., Oyake, A., Nguyen, H., Pace, T., Painter, T. H., Pempejian, J., Garcia-Pando, C. P., Pham, T., Phillips, B., Pollock, R., Purcell, R., Realmuto, V., Schoolcraft, J., Sen, A., Shin, S., Shaw, L., Soriano, M., Swayze, G., Thingvold, E., Vaid, A., and Zan, J.: The Earth Surface Mineral Dust Source Investigation: An Earth Science Imaging Spectroscopy Mission, in: 2020 IEEE Aerospace Conference, 2020 IEEE Aerospace Conference, 1–15, https://doi.org/10.1109/AERO47225.2020.9172731, 2020.

Grogan, D. F. P., Nathan, T. R., and Chen, S.-H.: Saharan Dust and the Nonlinear Evolution of the African Easterly Jet–African Easterly Wave System, J. Atmospheric Sci., 74, 27–47, https://doi.org/10.1175/JAS-D-16-0118.1, 2017.

Groß, S., Freudenthaler, V., Schepanski, K., Toledano, C., Schäfler, A., Ansmann, A., and Weinzierl, B.: Optical properties of long-range transported Saharan dust over Barbados as measured by dual-wavelength depolarization Raman lidar measurements, Atmospheric Chem. Phys., 15, 11067–11080, https://doi.org/10.5194/acp-15-11067-2015, 2015.

Gyan, K., Henry, W., Lacaille, S., Laloo, A., Lamsee-Ebanks, C., McKay, S., Antoine, R. M., and Monteil, M. A.: African dust clouds are associated with increased paediatric asthma accident and emergency admissions on the Caribbean island of Trinidad, Int. J. Biometeorol., 49, 371–376, https://doi.org/10.1007/s00484-005-0257-3, 2005.

Haarig, M., Ansmann, A., Althausen, D., Klepel, A., Groß, S., Freudenthaler, V., Toledano, C., Mamouri, R.-E., Farrell, D. A., Prescod, D. A., Marinou, E., Burton, S. P., Gasteiger, J., Engelmann, R., and Baars, H.: Triple-wavelength depolarization-ratio profiling of Saharan dust over Barbados during SALTRACE in 2013 and 2014, Atmospheric Chem. Phys., 17, 10767–10794, https://doi.org/10.5194/acp-17-10767-2017, 2017.

Hansell, R. A., Tsay, S. C., Ji, Q., Hsu, N. C., Jeong, M. J., Wang, S. H., Reid, J. S., Liou, K. N., and Ou, S. C.: An Assessment of the Surface Longwave Direct Radiative Effect of Airborne Saharan Dust during the NAMMA Field Campaign, J. Atmospheric Sci., 67, 1048–1065, https://doi.org/10.1175/2009JAS3257.1, 2010.

Haywood, J., Francis, P., Osborne, S., Glew, M., Loeb, N., Highwood, E., Tanré, D., Myhre, G., Formenti, P., and Hirst, E.: Radiative properties and direct radiative effect of Saharan dust measured by the C-130 aircraft during SHADE: 1. Solar spectrum, J. Geophys. Res. Atmospheres, 108, https://doi.org/10.1029/2002JD002687, 2003.

Haywood, J. M., Francis, P. N., Glew, M. D., and Taylor, J. P.: Optical properties and direct radiative effect of Saharan dust: A case study of two Saharan dust outbreaks using aircraft data, J. Geophys. Res. Atmospheres, 106, 18417–18430, https://doi.org/10.1029/2000JD900319, 2001.

Helgren, D. M. and Prospero, J. M.: Wind Velocities Associated with Dust Deflation Events in the Western Sahara, J. Appl. Meteorol. Climatol., 26, 1147–1151, https://doi.org/10.1175/1520-0450(1987)026<1147:WVAWDD>2.0.CO;2, 1987.

Hersbach, H., Bell, B., Berrisford, P., Hirahara, S., Horányi, A., Muñoz-Sabater, J., Nicolas, J., Peubey, C., Radu, R., Schepers, D., Simmons, A., Soci, C., Abdalla, S., Abellan, X., Balsamo, G., Bechtold, P., Biavati, G., Bidlot, J., Bonavita, M., De Chiara, G., Dahlgren, P., Dee, D., Diamantakis, M., Dragani, R., Flemming, J., Forbes, R., Fuentes, M., Geer, A., Haimberger, L., Healy, S., Hogan, R. J., Hólm, E., Janisková, M., Keeley, S., Laloyaux, P., Lopez, P., Lupu, C., Radnoti, G., de Rosnay, P.,

Rozum, I., Vamborg, F., Villaume, S., and Thépaut, J.-N.: The ERA5 global reanalysis, Q. J. R. Meteorol. Soc., 146, 1999–2049, https://doi.org/10.1002/qj.3803, 2020.

Highwood, E. J., Haywood, J. M., Silverstone, M. D., Newman, S. M., and Taylor, J. P.: Radiative properties and direct effect of Saharan dust measured by the C-130 aircraft during Saharan Dust Experiment (SHADE): 2. Terrestrial spectrum, J. Geophys. Res. Atmospheres, 108, https://doi.org/10.1029/2002JD002552, 2003.

Holben, B. N., Eck, T. F., Slutsker, I., Tanré, D., Buis, J. P., Setzer, A., Vermote, E., Reagan, J. A., Kaufman, Y. J., Nakajima, T., Lavenu, F., Jankowiak, I., and Smirnov, A.: AERONET—A Federated Instrument Network and Data Archive for Aerosol Characterization, Remote Sens. Environ., 66, 1–16, https://doi.org/10.1016/S0034-4257(98)00031-5, 1998.

Holben, B. N., Tanré, D., Smirnov, A., Eck, T. F., Slutsker, I., Abuhassan, N., Newcomb, W. W., Schafer, J. S., Chatenet, B., Lavenu, F., Kaufman, Y. J., Castle, J. V., Setzer, A., Markham, B., Clark, D., Frouin, R., Halthore, R., Karneli, A., O'Neill, N. T., Pietras, C., Pinker, R. T., Voss, K., and Zibordi, G.: An emerging ground-based aerosol climatology: Aerosol optical depth from AERONET, J. Geophys. Res. Atmospheres, 106, 12067–12097, https://doi.org/10.1029/2001JD900014, 2001.

Hsu, N. C., Lee, J., Sayer, A. M., Kim, W., Bettenhausen, C., and Tsay, S. -C.: VIIRS Deep Blue Aerosol Products Over Land: Extending the EOS Long-Term Aerosol Data Records, J. Geophys. Res. Atmospheres, 124, 4026–4053, https://doi.org/10.1029/2018JD029688, 2019.

Huang, J., Zhang, C., and Prospero, J. M.: African dust outbreaks: A satellite perspective of temporal and spatial variability over the tropical Atlantic Ocean, J. Geophys. Res. Atmospheres, 115, https://doi.org/10.1029/2009JD012516, 2010.

Huneeus, N., Schulz, M., Balkanski, Y., Griesfeller, J., Prospero, J., Kinne, S., Bauer, S., Boucher, O., Chin, M., Dentener, F., Diehl, T., Easter, R., Fillmore, D., Ghan, S., Ginoux, P., Grini, A., Horowitz, L., Koch, D., Krol, M. C., Landing, W., Liu, X., Mahowald, N., Miller, R., Morcrette, J.-J., Myhre, G., Penner, J., Perlwitz, J., Stier, P., Takemura, T., and Zender, C. S.: Global dust model intercomparison in AeroCom phase I, Atmospheric Chem. Phys., 11, 7781–7816, https://doi.org/10.5194/acp-11-7781-2011, 2011.

Jenkins, G. S., Pratt, A. S., and Heymsfield, A.: Possible linkages between Saharan dust and tropical cyclone rain band invigoration in the eastern Atlantic during NAMMA-06, Geophys. Res. Lett., 35, https://doi.org/10.1029/2008GL034072, 2008.

Jickells, T. D., Baker, A. R., and Chance, R.: Atmospheric transport of trace elements and nutrients to the oceans, Philos. Trans. R. Soc. Math. Phys. Eng. Sci., 374, 20150286, https://doi.org/10.1098/rsta.2015.0286, 2016.

Johnson, G. C., Lyman, J. M., and Loeb, N. G.: Improving estimates of Earth's energy imbalance, Nat. Clim. Change, 6, 639–640, https://doi.org/10.1038/nclimate3043, 2016.

Jones, C., Mahowald, N., and Luo, C.: The role of easterly waves on African desert dust transport, J. Clim., 16, 3617–3628, https://doi.org/10.1175/1520-0442(2003)016<3617:TROEWO>2.0.CO;2, 2003.

Kalashnikova, O. V. and Kahn, R. A.: Mineral dust plume evolution over the Atlantic from MISR and MODIS aerosol retrievals, J. Geophys. Res. Atmospheres, 113, https://doi.org/10.1029/2008JD010083, 2008.

Kanitz, T., Engelmann, R., Heinold, B., Baars, H., Skupin, A., and Ansmann, A.: Tracking the Saharan Air Layer with shipborne lidar across the tropical Atlantic, Geophys. Res. Lett., 41, 1044–1050, https://doi.org/10.1002/2013GL058780, 2014.

Kar, J., Vaughan, M. A., Lee, K.-P., Tackett, J. L., Avery, M. A., Garnier, A., Getzewich, B. J., Hunt, W. H., Josset, D., Liu, Z., Lucker, P. L., Magill, B., Omar, A. H., Pelon, J., Rogers, R. R., Toth, T. D., Trepte, C. R., Vernier, J.-P., Winker, D. M., and Young, S. A.: CALIPSO lidar calibration at 532nm: version 4 nighttime algorithm, Atmospheric Meas. Tech., 11, 1459–1479, https://doi.org/10.5194/amt-11-1459-2018, 2018.

Karyampudi, V. M. and Carlson, T. N.: Analysis and Numerical Simulations of the Saharan Air Layer and Its Effect on Easterly Wave Disturbances, J. Atmospheric Sci., 45, 3102–3136, https://doi.org/10.1175/1520-0469(1988)045<3102:AANSOT>2.0.CO;2, 1988.

Kato, S., Rose, F. G., Rutan, D. A., Thorsen, T. J., Loeb, N. G., Doelling, D. R., Huang, X., Smith, W. L., Su, W., and Ham, S.-H.: Surface Irradiances of Edition 4.0 Clouds and the Earth's Radiant Energy System (CERES) Energy Balanced and Filled (EBAF) Data Product, J. Clim., 31, 4501–4527, https://doi.org/10.1175/JCLI-D-17-0523.1, 2018.

Kaufman, Y. J., Koren, I., Remer, L. A., Tanré, D., Ginoux, P., and Fan, S.: Dust transport and deposition observed from the Terra-Moderate Resolution Imaging Spectroradiometer (MODIS) spacecraft over the Atlantic Ocean, J. Geophys. Res. Atmospheres, 110, https://doi.org/10.1029/2003JD004436, 2005.

Kim, D., Chin, M., Remer, L. A., Diehl, T., Bian, H., Yu, H., Brown, M. E., and Stockwell, W. R.: Role of surface wind and vegetation cover in multi-decadal variations of dust emission in the Sahara and Sahel, Atmos. Environ., 148, 282–296, https://doi.org/10.1016/j.atmosenv.2016.10.051, 2017.

Kim, M.-H., Omar, A. H., Tackett, J. L., Vaughan, M. A., Winker, D. M., Trepte, C. R., Hu, Y., Liu, Z., Poole, L. R., Pitts, M. C., Kar, J., and Magill, B. E.: The CALIPSO version 4 automated aerosol classification and lidar ratio selection algorithm, Atmospheric Meas. Tech., 11, 6107–6135, https://doi.org/10.5194/amt-11-6107-2018, 2018.

Knippertz, P. and Fink, A. H.: Synoptic and dynamic aspects of an extreme springtime Saharan dust outbreak, Q. J. R. Meteorol. Soc., 132, 1153–1177, https://doi.org/10.1256/qj.05.109, 2006.

Knippertz, P. and Todd, M. C.: Mineral dust aerosols over the Sahara: Meteorological controls on emission and transport and implications for modeling, Rev. Geophys., 50, https://doi.org/10.1029/2011RG000362, 2012.

Kok, J. F., Ridley, D. A., Zhou, Q., Miller, R. L., Zhao, C., Heald, C. L., Ward, D. S., Albani, S., and Haustein, K.: Smaller desert dust cooling effect estimated from analysis of dust size and abundance, Nat. Geosci., 10, 274–278, https://doi.org/10.1038/ngeo2912, 2017.

Kok, J. F., Adebiyi, A. A., Albani, S., Balkanski, Y., Checa-Garcia, R., Chin, M., Colarco, P. R., Hamilton, D. S., Huang, Y., Ito, A., Klose, M., Li, L., Mahowald, N. M., Miller, R. L., Obiso, V., Pérez García-Pando, C., Rocha-Lima, A., and Wan, J. S.: Contribution of the world's main dust source regions to the global cycle of desert dust, Atmospheric Chem. Phys., 21, 8169–8193, https://doi.org/10.5194/acp-21-8169-2021, 2021.

Kok, J. F., Storelvmo, T., Karydis, V. A., Adebiyi, A. A., Mahowald, N. M., Evan, A. T., He, C., and Leung, D. M.: Mineral dust aerosol impacts on global climate and climate change, Nat. Rev. Earth Environ., 4, 71–86, https://doi.org/10.1038/s43017-022-00379-5, 2023.

Kumar, A., Abouchami, W., Galer, S. J. G., Garrison, V. H., Williams, E., and Andreae, M. O.: A radiogenic isotope tracer study of transatlantic dust transport from Africa to the Caribbean, Atmos. Environ., 82, 130–143, https://doi.org/10.1016/j.atmosenv.2013.10.021, 2014.

Largeron, Y., Guichard, F., Bouniol, D., Couvreux, F., Kergoat, L., and Marticorena, B.: Can we use surface wind fields from meteorological reanalyses for Sahelian dust emission simulations?, Geophys. Res. Lett., 42, 2490–2499, https://doi.org/10.1002/2014GL062938, 2015.

Lensky, I. M. and Rosenfeld, D.: Clouds-Aerosols-Precipitation Satellite Analysis Tool (CAPSAT), Atmospheric Chem. Phys., 8, 6739–6753, https://doi.org/10.5194/acp-8-6739-2008, 2008.

Leroux, S. and Hall, N. M. J.: On the Relationship between African Easterly Waves and the African Easterly Jet, J. Atmospheric Sci., 66, 2303–2316, https://doi.org/10.1175/2009JAS2988.1, 2009.

Levin, Z., Ganor, E., and Gladstein, V.: The Effects of Desert Particles Coated with Sulfate on Rain Formation in the Eastern Mediterranean, J. Appl. Meteorol. Climatol., 35, 1511–1523, https://doi.org/10.1175/1520-0450(1996)035<1511:TEODPC>2.0.CO;2, 1996.

Li, F., Vogelmann, A. M., and Ramanathan, V.: Saharan Dust Aerosol Radiative Forcing Measured from Space, J. Clim., 17, 2558–2571, https://doi.org/10.1175/1520-0442(2004)017<2558:SDARFM>2.0.CO;2, 2004.

Li, F., Ginoux, P., and Ramaswamy, V.: Transport of Patagonian dust to Antarctica, J. Geophys. Res. Atmospheres, 115, https://doi.org/10.1029/2009JD012356, 2010.

Li, J., Garshick, E., Huang, S., and Koutrakis, P.: Impacts of El Niño-Southern Oscillation on surface dust levels across the world during 1982–2019, Sci. Total Environ., 769, 144566, https://doi.org/10.1016/j.scitotenv.2020.144566, 2021.

Li, W., Li, L., Fu, R., Deng, Y., and Wang, H.: Changes to the North Atlantic Subtropical High and Its Role in the Intensification of Summer Rainfall Variability in the Southeastern United States, J. Clim., 24, 1499–1506, https://doi.org/10.1175/2010JCLI3829.1, 2011.

Liu, H., Remer, L. A., Huang, J., Huang, H.-C., Kondragunta, S., Laszlo, I., Oo, M., and Jackson, J. M.: Preliminary evaluation of S-NPP VIIRS aerosol optical thickness, J. Geophys. Res. Atmospheres, 119, 3942–3962, https://doi.org/10.1002/2013JD020360, 2014.

Loeb, N. G., Doelling, D. R., Wang, H., Su, W., Nguyen, C., Corbett, J. G., Liang, L., Mitrescu, C., Rose, F. G., and Kato, S.: Clouds and the Earth's Radiant Energy System (CERES) Energy Balanced and Filled (EBAF) Top-of-Atmosphere (TOA) Edition-4.0 Data Product, J. Clim., 31, 895–918, https://doi.org/10.1175/JCLI-D-17-0208.1, 2018.

Mahowald, N., Albani, S., Kok, J. F., Engelstaeder, S., Scanza, R., Ward, D. S., and Flanner, M. G.: The size distribution of desert dust aerosols and its impact on the Earth system, Aeolian Res., 15, 53–71, https://doi.org/10.1016/j.aeolia.2013.09.002, 2014.

Marsham, J. H., Parker, D. J., Grams, C. M., Taylor, C. M., and Haywood, J. M.: Uplift of Saharan dust south of the intertropical discontinuity, J. Geophys. Res. Atmospheres, 113, https://doi.org/10.1029/2008JD009844, 2008.

Martin, E. R. and Schumacher, C.: The Caribbean Low-Level Jet and Its Relationship with Precipitation in IPCC AR4 Models, J. Clim., 24, 5935–5950, https://doi.org/10.1175/JCLI-D-11-00134.1, 2011.

Martínez, M. A., Ruiz, J., and Cuevas, E.: Use of SEVIRI images and derived products in a WMO Sand and dust Storm Warning System, IOP Conf. Ser. Earth Environ. Sci., 7, 012004, https://doi.org/10.1088/1755-1307/7/1/012004, 2009.

Mehra, M., Shrestha, S., Ap, K., Guagenti, M., Moffett, C. E., VerPloeg, S. G., Coogan, M. A., Rai, M., Kumar, R., Andrews, E., Sherman, J. P., Flynn III, J. H., Usenko, S., and Sheesley, R. J.: Atmospheric heating in the US from saharan dust: Tracking

the June 2020 event with surface and satellite observations, Atmos. Environ., 310, 119988, https://doi.org/10.1016/j.atmosenv.2023.119988, 2023.

Meloni, D., di Sarra, A., Di Iorio, T., and Fiocco, G.: Influence of the vertical profile of Saharan dust on the visible direct radiative forcing, J. Quant. Spectrosc. Radiat. Transf., 93, 397–413, https://doi.org/10.1016/j.jqsrt.2004.08.035, 2005.

MODIS Land General Accuracy Statement: https://modis-land.gsfc.nasa.gov/ValStatus.php?ProductID=MOD13, last access: 30 March 2024, last update: 2023.

Moulin, C. and Chiapello, I.: Evidence of the control of summer atmospheric transport of African dust over the Atlantic by Sahel sources from TOMS satellites (1979–2000), Geophys. Res. Lett., 31, https://doi.org/10.1029/2003GL018931, 2004.

Moulin, C., Lambert, C. E., Dulac, F., and Dayan, U.: Control of atmospheric export of dust from North Africa by the North Atlantic Oscillation, Nature, 387, 691–694, https://doi.org/10.1038/42679, 1997.

Muñoz-Sabater, J., Dutra, E., Agustí-Panareda, A., Albergel, C., Arduini, G., Balsamo, G., Boussetta, S., Choulga, M., Harrigan, S., Hersbach, H., Martens, B., Miralles, D. G., Piles, M., Rodríguez-Fernández, N. J., Zsoter, E., Buontempo, C., and Thépaut, J.-N.: ERA5-Land: a state-of-the-art global reanalysis dataset for land applications, Earth Syst. Sci. Data, 13, 4349–4383, https://doi.org/10.5194/essd-13-4349-2021, 2021.

Myhre, G., Grini, A., Haywood, J. M., Stordal, F., Chatenet, B., Tanré, D., Sundet, J. K., and Isaksen, I. S. A.: Modeling the radiative impact of mineral dust during the Saharan Dust Experiment (SHADE) campaign, J. Geophys. Res. Atmospheres, 108, https://doi.org/10.1029/2002JD002566, 2003.

Okin, G. S., Mahowald, N., Chadwick, O. A., and Artaxo, P.: Impact of desert dust on the biogeochemistry of phosphorus in terrestrial ecosystems, Glob. Biogeochem. Cycles, 18, https://doi.org/10.1029/2003GB002145, 2004.

Ott, S.-T., Ott, A., Martin, D. W., and Young, J. A.: Analysis of a Trans-Atlantic Saharan Dust Outbreak Based on Satellite and GATE Data, Mon. Weather Rev., 119, 1832–1850, https://doi.org/10.1175/1520-0493(1991)119<1832:AOATAS>2.0.CO;2, 1991.

Pan, W., Wu, L., and Shie, C.-L.: Influence of the Saharan Air Layer on Atlantic tropical cyclone formation during the period 1–12 September 2003, Adv. Atmospheric Sci., 28, 16–32, https://doi.org/10.1007/s00376-010-9165-5, 2011.

Petit, R. H., Legrand, M., Jankowiak, I., Molinié, J., Asselin de Beauville, C., Marion, G., and Mansot, J. L.: Transport of Saharan dust over the Caribbean Islands: Study of an event, J. Geophys. Res. Atmospheres, 110, https://doi.org/10.1029/2004JD004748, 2005.

Piles, M., Ballabrera-Poy, J., and Muñoz-Sabater, J.: Dominant Features of Global Surface Soil Moisture Variability Observed by the SMOS Satellite, Remote Sens., 11, 95, https://doi.org/10.3390/rs11010095, 2019.

Prenni, A. J., Petters, M. D., Faulhaber, A., Carrico, C. M., Ziemann, P. J., Kreidenweis, S. M., and DeMott, P. J.: Heterogeneous ice nucleation measurements of secondary organic aerosol generated from ozonolysis of alkenes, Geophys. Res. Lett., 36, https://doi.org/10.1029/2008GL036957, 2009.

Prospero, J. M.: Long-term measurements of the transport of African mineral dust to the southeastern United States: Implications for regional air quality, J. Geophys. Res. Atmospheres, 104, 15917–15927, https://doi.org/10.1029/1999JD900072, 1999.

Prospero, J. M. and Carlson, T. N.: Radon-222 in the North Atlantic Trade Winds: Its Relationship to Dust Transport from Africa, Science, 167, 974–977, https://doi.org/10.1126/science.167.3920.974, 1970.

Prospero, J. M. and Carlson, T. N.: Vertical and areal distribution of Saharan dust over the western equatorial north Atlantic Ocean, J. Geophys. Res. 1896-1977, 77, 5255–5265, https://doi.org/10.1029/JC077i027p05255, 1972.

Prospero, J. M. and Carlson, T. N.: Saharan air outbreaks over the tropical North Atlantic, Pure Appl. Geophys. PAGEOPH, 119, 677–691, https://doi.org/10.1007/BF00878167, 1981.

Prospero, J. M. and Lamb, P. J.: African Droughts and Dust Transport to the Caribbean: Climate Change Implications, Science, 302, 1024–1027, https://doi.org/10.1126/science.1089915, 2003.

Prospero, J. M., Bonatti, E., Schubert, C., and Carlson, T. N.: Dust in the Caribbean atmosphere traced to an African dust storm, Earth Planet. Sci. Lett., 9, 287–293, https://doi.org/10.1016/0012-821X(70)90039-7, 1970.

Prospero, J. M., Ginoux, P., Torres, O., Nicholson, S. E., and Gill, T. E.: Environmental Characterization of Global Sources of Atmospheric Soil Dust Identified with the Nimbus 7 Total Ozone Mapping Spectrometer (toms) Absorbing Aerosol Product, Rev. Geophys., 40, 2-1-2–31, https://doi.org/10.1029/2000RG000095, 2002.

Prospero, J. M., Blades, E., Mathison, G., and Naidu, R.: Interhemispheric transport of viable fungi and bacteria from Africa to the Caribbean with soil dust, Aerobiologia, 21, 1–19, https://doi.org/10.1007/s10453-004-5872-7, 2005.

Prospero, J. M., Delany, A. C., Delany, A. C., and Carlson, T. N.: The Discovery of African Dust Transport to the Western Hemisphere and the Saharan Air Layer: A History, Bull. Am. Meteorol. Soc., 102, E1239–E1260, https://doi.org/10.1175/BAMS-D-19-0309.1, 2021.

Pu, B. and Ginoux, P.: Climatic factors contributing to long-term variations in surface fine dust concentration in the United States, Atmospheric Chem. Phys., 18, 4201–4215, https://doi.org/10.5194/acp-18-4201-2018, 2018a.

Pu, B. and Ginoux, P.: How reliable are CMIP5 models in simulating dust optical depth?, Atmospheric Chem. Phys., 18, 12491–12510, https://doi.org/10.5194/acp-18-12491-2018, 2018b.

Pu, B. and Jin, Q.: A Record-Breaking Trans-Atlantic African Dust Plume Associated with Atmospheric Circulation Extremes in June 2020, Bull. Am. Meteorol. Soc., 102, E1340–E1356, https://doi.org/10.1175/BAMS-D-21-0014.1, 2021.

Pu, B., Ginoux, P., Guo, H., Hsu, N. C., Kimball, J., Marticorena, B., Malyshev, S., Naik, V., O'Neill, N. T., Pérez García-Pando, C., Paireau, J., Prospero, J. M., Shevliakova, E., and Zhao, M.: Retrieving the global distribution of the threshold of wind erosion from satellite data and implementing it into the Geophysical Fluid Dynamics Laboratory land–atmosphere model (GFDL AM4.0/LM4.0), Atmospheric Chem. Phys., 20, 55–81, https://doi.org/10.5194/acp-20-55-2020, 2020.

Randles, C. A., Silva, A. M. da, Buchard, V., Colarco, P. R., Darmenov, A., Govindaraju, R., Smirnov, A., Holben, B., Ferrare, R., Hair, J., Shinozuka, Y., and Flynn, C. J.: The MERRA-2 Aerosol Reanalysis, 1980 Onward. Part I: System Description and Data Assimilation Evaluation, J. Clim., 30, 6823–6850, https://doi.org/10.1175/JCLI-D-16-0609.1, 2017.

Reale, O., Lau, K. M., and Silva, A. da: Impact of Interactive Aerosol on the African Easterly Jet in the NASA GEOS-5 Global Forecasting System, Weather Forecast., 26, 504–519, https://doi.org/10.1175/WAF-D-10-05025.1, 2011.

Reddy, K., Kumar, D. V. P., Ahammed, Y. N., and Naja, M.: Aerosol vertical profiles strongly affect their radiative forcing uncertainties: study by using ground-based lidar and other measurements, Remote Sens. Lett., 4, 1018–1027, https://doi.org/10.1080/2150704X.2013.828182, 2013.

Roberts, A. J., Woodage, M. J., Marsham, J. H., Highwood, E. J., Ryder, C. L., McGinty, W., Wilson, S., and Crook, J.: Can explicit convection improve modelled dust in summertime West Africa?, Atmospheric Chem. Phys., 18, 9025–9048, https://doi.org/10.5194/acp-18-9025-2018, 2018.

Rosenfeld, D., Rudich, Y., and Lahav, R.: Desert dust suppressing precipitation: A possible desertification feedback loop, Proc. Natl. Acad. Sci., 98, 5975–5980, https://doi.org/10.1073/pnas.101122798, 2001.

Rutan, D. A., Kato, S., Doelling, D. R., Rose, F. G., Nguyen, L. T., Caldwell, T. E., and Loeb, N. G.: CERES Synoptic Product: Methodology and Validation of Surface Radiant Flux, J. Atmospheric Ocean. Technol., 32, 1121–1143, https://doi.org/10.1175/JTECH-D-14-00165.1, 2015.

Sassen, K.: The Polarization Lidar Technique for Cloud Research: A Review and Current Assessment, Bull. Am. Meteorol. Soc., 72, 1848–1866, https://doi.org/10.1175/1520-0477(1991)072<1848:TPLTFC>2.0.CO;2, 1991.

Sayer, A. M., Hsu, N. C., Lee, J., Kim, W. V., and Dutcher, S. T.: Validation, Stability, and Consistency of MODIS Collection 6.1 and VIIRS Version 1 Deep Blue Aerosol Data Over Land, J. Geophys. Res. Atmospheres, 124, 4658–4688, https://doi.org/10.1029/2018JD029598, 2019.

Schepanski, K.: Transport of Mineral Dust and Its Impact on Climate, Geosciences, 8, 151, https://doi.org/10.3390/geosciences8050151, 2018.

Schepanski, K., Tegen, I., Laurent, B., Heinold, B., and Macke, A.: A new Saharan dust source activation frequency map derived from MSG-SEVIRI IR-channels, Geophys. Res. Lett., 34, https://doi.org/10.1029/2007GL030168, 2007.

Schepanski, K., Heinold, B., and Tegen, I.: Harmattan, Saharan heat low, and West African monsoon circulation: modulations on the Saharan dust outflow towards the North Atlantic, Atmospheric Chem. Phys., 17, 10223–10243, https://doi.org/10.5194/acp-17-10223-2017, 2017.

Schmetz, J., Pili, P., Tjemkes, S., Just, D., Kerkmann, J., Rota, S., and Ratier, A.: AN INTRODUCTION TO METEOSAT SECOND GENERATION (MSG), Bull. Am. Meteorol. Soc., 83, 977–992, https://doi.org/10.1175/1520-0477(2002)083<0977:AITMSG>2.3.CO;2, 2002.

Scott, S. R., Dunion, J. P., Olson, M. L., and Gay, D. A.: Lead Isotopes in North American Precipitation Record the Presence of Saharan Dust, Bull. Am. Meteorol. Soc., 103, E281–E292, https://doi.org/10.1175/BAMS-D-20-0212.1, 2022.

Shinn, E. A., Griffin, D. W., and Seba, D. B.: Atmospheric Transport of Mold Spores in Clouds of Desert Dust, Arch. Environ. Health, 58, 498–504, 2003.

Slingo, A., Ackerman, T. P., Allan, R. P., Kassianov, E. I., McFarlane, S. A., Robinson, G. J., Barnard, J. C., Miller, M. A., Harries, J. E., Russell, J. E., and Dewitte, S.: Observations of the impact of a major Saharan dust storm on the atmospheric radiation balance, Geophys. Res. Lett., 33, https://doi.org/10.1029/2006GL027869, 2006.

Song, Q., Zhang, Z., Yu, H., Kato, S., Yang, P., Colarco, P., Remer, L. A., and Ryder, C. L.: Net radiative effects of dust in the tropical North Atlantic based on integrated satellite observations and in situ measurements, Atmospheric Chem. Phys., 18, 11303–11322, https://doi.org/10.5194/acp-18-11303-2018, 2018.

Strong, J. D. O., Vecchi, G. A., and Ginoux, P.: The Climatological Effect of Saharan Dust on Global Tropical Cyclones in a Fully Coupled GCM, J. Geophys. Res. Atmospheres, 123, 5538–5559, https://doi.org/10.1029/2017JD027808, 2018.

Tegen, I. and Lacis, A. A.: Modeling of particle size distribution and its influence on the radiative properties of mineral dust aerosol, J. Geophys. Res. Atmospheres, 101, 19237–19244, https://doi.org/10.1029/95JD03610, 1996.

Tegen, I., Lacis, A. A., and Fung, I.: The influence on climate forcing of mineral aerosols from disturbed soils, Nature, 380, 419–422, https://doi.org/10.1038/380419a0, 1996.

Tegen, I., Bierwirth, E., Heinold, B., Helmert, J., and Wendisch, M.: Effect of measured surface albedo on modeled Saharan dust solar radiative forcing, J. Geophys. Res. Atmospheres, 115, https://doi.org/10.1029/2009JD013764, 2010.

Tindan, J. Z., Jin, Q., and Pu, B.: Understanding day–night differences in dust aerosols over the dust belt of North Africa, the Middle East, and Asia, Atmospheric Chem. Phys., 23, 5435–5466, https://doi.org/10.5194/acp-23-5435-2023, 2023.

Villar-Argaiz, M., Cabrerizo, M. J., González-Olalla, J. M., Valiñas, M. S., Rajic, S., and Carrillo, P.: Growth impacts of Saharan dust, mineral nutrients, and CO2 on a planktonic herbivore in southern Mediterranean lakes, Sci. Total Environ., 639, 118–128, https://doi.org/10.1016/j.scitotenv.2018.05.041, 2018.

Vuolo, M. R., Chepfer, H., Menut, L., and Cesana, G.: Comparison of mineral dust layers vertical structures modeled with CHIMERE-DUST and observed with the CALIOP lidar, J. Geophys. Res. Atmospheres, 114, https://doi.org/10.1029/2008JD011219, 2009.

Wang, C.: Variability of the Caribbean Low-Level Jet and its relations to climate, Clim. Dyn., 29, 411–422, https://doi.org/10.1007/s00382-007-0243-z, 2007.

Wang, C., Dong, S., Evan, A. T., Foltz, G. R., and Lee, S.-K.: Multidecadal Covariability of North Atlantic Sea Surface Temperature, African Dust, Sahel Rainfall, and Atlantic Hurricanes, J. Clim., 25, 5404–5415, https://doi.org/10.1175/JCLI-D-11-00413.1, 2012.

Wang, J., Petersen, W. A., and Wolff, D. B.: Validation of Satellite-Based Precipitation Products from TRMM to GPM, Remote Sens., 13, 1745, https://doi.org/10.3390/rs13091745, 2021.

Wang, Z., Zhong, R., Lai, C., and Chen, J.: Evaluation of the GPM IMERG satellite-based precipitation products and the hydrological utility, Atmospheric Res., 196, 151–163, https://doi.org/10.1016/j.atmosres.2017.06.020, 2017.

Waters, S. M., Purdue, S. K., Armstrong, R., and Detrés, Y.: Metagenomic investigation of African dust events in the Caribbean, FEMS Microbiol. Lett., 367, fnaa051, https://doi.org/10.1093/femsle/fnaa051, 2020.

Weinzierl, B., Ansmann, A., Prospero, J. M., Althausen, D., Benker, N., Chouza, F., Dollner, M., Farrell, D., Fomba, W. K., Freudenthaler, V., Gasteiger, J., Groß, S., Haarig, M., Heinold, B., Kandler, K., Kristensen, T. B., Mayol-Bracero, O. L., Müller, T., Reitebuch, O., Sauer, D., Schäfler, A., Schepanski, K., Spanu, A., Tegen, I., Toledano, C., and Walser, A.: The Saharan Aerosol Long-Range Transport and Aerosol–Cloud-Interaction Experiment: Overview and Selected Highlights, Bull. Am. Meteorol. Soc., 98, 1427–1451, https://doi.org/10.1175/BAMS-D-15-00142.1, 2017.

Wielicki, B. A., Barkstrom, B. R., Harrison, E. F., Lee, R. B., Smith, G. L., and Cooper, J. E.: Clouds and the Earth's Radiant Energy System (CERES): An Earth Observing System Experiment, Bull. Am. Meteorol. Soc., 77, 853–868, https://doi.org/10.1175/1520-0477(1996)077<0853:CATERE>2.0.CO;2, 1996.

Wilcox, E. M., Lau, K. M., and Kim, K.-M.: A northward shift of the North Atlantic Ocean Intertropical Convergence Zone in response to summertime Saharan dust outbreaks, Geophys. Res. Lett., 37, https://doi.org/10.1029/2009GL041774, 2010.

Winker, D. M., Hunt, W. H., and Hostetler, C. A.: Status and performance of the CALIOP lidar, in: Laser Radar Techniques for Atmospheric Sensing, Laser Radar Techniques for Atmospheric Sensing, 8–15, https://doi.org/10.1117/12.571955, 2004.

Winker, D. M., Hunt, W. H., and McGill, M. J.: Initial performance assessment of CALIOP, Geophys. Res. Lett., 34, https://doi.org/10.1029/2007GL030135, 2007.

Wu, C., Lin, Z., and Liu, X.: The global dust cycle and uncertainty in CMIP5 (Coupled Model Intercomparison Project phase 5) models, Atmospheric Chem. Phys., 20, 10401–10425, https://doi.org/10.5194/acp-20-10401-2020, 2020.

Xu, H., Guo, J., Wang, Y., Zhao, C., Zhang, Z., Min, M., Miao, Y., Liu, H., He, J., Zhou, S., and Zhai, P.: Warming effect of dust aerosols modulated by overlapping clouds below, Atmos. Environ., 166, 393–402, https://doi.org/10.1016/j.atmosenv.2017.07.036, 2017.

Yin, Z.-Y., Maytubby, A., and Liu, X.: Variation Patterns of the ENSO's Effects on Dust Activity in North Africa, Arabian Peninsula, and Central Asia of the Dust Belt, Climate, 10, 150, https://doi.org/10.3390/cli10100150, 2022.

Yorks, J. E., McGill, M., Rodier, S., Vaughan, M., Hu, Y., and Hlavka, D.: Radiative effects of African dust and smoke observed from Clouds and the Earth's Radiant Energy System (CERES) and Cloud-Aerosol Lidar with Orthogonal Polarization (CALIOP) data, J. Geophys. Res.-Atmospheres, 114, D00H04, https://doi.org/10.1029/2009JD012000, 2009.

Yu, H., Kaufman, Y. J., Chin, M., Feingold, G., Remer, L. A., Anderson, T. L., Balkanski, Y., Bellouin, N., Boucher, O., Christopher, S., DeCola, P., Kahn, R., Koch, D., Loeb, N., Reddy, M. S., Schulz, M., Takemura, T., and Zhou, M.: A review of measurement-based assessments of the aerosol direct radiative effect and forcing, Atmospheric Chem. Phys., 6, 613–666, https://doi.org/10.5194/acp-6-613-2006, 2006.

Yu, H., Chin, M., Bian, H., Yuan, T., Prospero, J. M., Omar, A. H., Remer, L. A., Winker, D. M., Yang, Y., Zhang, Y., and Zhang, Z.: Quantification of trans-Atlantic dust transport from seven-year (2007–2013) record of CALIPSO lidar measurements, Remote Sens. Environ., 159, 232–249, https://doi.org/10.1016/j.rse.2014.12.010, 2015a.

Yu, H., Chin, M., Yuan, T., Bian, H., Remer, L. A., Prospero, J. M., Omar, A., Winker, D., Yang, Y., Zhang, Y., Zhang, Z., and Zhao, C.: The fertilizing role of African dust in the Amazon rainforest: A first multiyear assessment based on data from Cloud-Aerosol Lidar and Infrared Pathfinder Satellite Observations, Geophys. Res. Lett., 42, 1984–1991, https://doi.org/10.1002/2015GL063040, 2015b.

Yu, H., Tan, Q., Chin, M., Remer, L. A., Kahn, R. A., Bian, H., Kim, D., Zhang, Z., Yuan, T., Omar, A. H., Winker, D. M., Levy, R. C., Kalashnikova, O., Crepeau, L., Capelle, V., and Chédin, A.: Estimates of African Dust Deposition Along the Trans-Atlantic Transit Using the Decadelong Record of Aerosol Measurements from CALIOP, MODIS, MISR, and IASI, J. Geophys. Res. Atmospheres, 124, 7975–7996, https://doi.org/10.1029/2019JD030574, 2019.

Yu, H., Tan, Q., Zhou, L., Zhou, Y., Bian, H., Chin, M., Ryder, C. L., Levy, R. C., Pradhan, Y., Shi, Y., Song, Q., Zhang, Z., Colarco, P. R., Kim, D., Remer, L. A., Yuan, T., Mayol-Bracero, O., and Holben, B. N.: Observation and modeling of the historic "Godzilla" African dust intrusion into the Caribbean Basin and the southern US in June 2020, Atmospheric Chem. Phys., 21, 12359–12383, https://doi.org/10.5194/acp-21-12359-2021, 2021.